July 2, 2023

BACHELOR ASSIGNMENT

The visualisation of permanent charges in electro-responsive, random co-polymer hydrogels with confocal laser scanning microscopy

Student: Xiaoyu Cao
Head supervisor: Sissi de Beer
Daily supervisor: Esli Diepenbroek
Biomolecular Nanotechnology (BNT)

UNIVERSITY OF TWENTE.

Acknowledgements

I acknowledge with gratitude to my head supervisor Sissi de Beer and daily supervisor Esli Diepenbroek, who have always been sincere and helpful in enabling me to complete the bachelor assignment on *The visualisation of permanent charges in electro-responsive, random co-polymer hydrogels with confocal laser scanning microscopy*.

I would also like to extend my gratitude to the staffs of Biomedical Nanotechnology (BNT) group and Team Sissi for providing me with all the facility that was required. I am grateful to all my families, friends and those with whom I have had the pleasure during this thesis.

The research has indeed helped me to explore knowledge avenues related to material science and I am sure it will help me in my future.

Abstract

A series of various monomers ratios between poly(3-sulfopropyl methacrylate)-*ran*-poly(hydroxyethyl methacrylate), p(SPMA)-*ran*-p(HEMA), hydrogels were synthesised by free radical polymerisation. The sulfonate group SO_3^- defined the anionic character of SPMA, and thus induced electric charges on the polymer backbone which subsequently the hydrogels are responsive to an electric field. A proof of concept for the use of CLSM to visualise the charge density distribution was performed. The hydrogels were characterised by swelling ratio, scanning electron microscopy (SEM), optical microscopy, Fourier transform infrared spectroscopy (FTIR) and confocal laser scanning microscopy. It was found 25% and 100% SPMA molar ratio yielded the highest swelling ratio, images acquired using optical microscope and SEM supported the results. FTIR detected the characteristic wavenumber of the SO_3^- group at 1040cm^{-1}, and the signal decreased along the SPMA molar ratio. Finally, the hydrogels were immersed in 0.1mM of Rhodamine B and characterised using CLSM. The acquired images showed an homogeneous electric charge density, and the light intensity decreased along the z-stack.

Contents

1 Introduction

Burning fossil fuels [1] as a source of energy supply began around the Industrial Revolution, whereby the amount of fossil fuels consumption reached 136,0TWh [1] in 2021. For a sustainable and green economy [2], the use of raw materials that originate from a renewable source is required to substitute the overwhelming consumption of fossil fuels. Concerning the economic and ecological aspects, scientists have put attention on biobased materials. Biobased materials [3, 4] are products derived from living matters, such as microorganisms and waste residues, and the source of the materials can be natural or synthesised. Despite the high potential of the biobased materials to neutralise the carbon footprint, they are not suitable for direct use due to the high fraction of moisture content which is larger than 60%wt.[3]. Therefore, drying process is needed to get rid of the high-level moisture content. Among various drying techniques, convective dryers [3, 5, 6] are most commonly used. There are several types of convective dryers, for example rotary drum dryers, fluidized bed dyers and conventional convective dryers. The dehydration principle [6, 7] is the product of heat and mass transport, and the water content is evaporated through the use hot air generated from a heat exchanger. Despite the fact that the convective heat flows are able to dry high water content of approximately 70% [6], there are several drawbacks including low thermal conductivity, extensive drying time and loss of materials during the performance. Moreover, the convective drying is energy intensive [3, 5], and the estimated specific energy consumption is 85.45 MJ [8, 9] per kilogram of water removed. The low efficiency of the drying process, and thus the large energy consumption compelled researchers to develop alternative technologies that is energy efficient and able to absorb large amount of moisture content.

Hydrogels [10–12], besides from their traditional biological applications, are emerging materials for applications related to energy and water treatment. For example, hydrogels are applied for solar desalination [13, 14]. The traditional usage of solar evaporation for water purification is rather slow process and low efficiency, hydrogels have the ability to uptake water which enhance the desalination process efficiency to 95% [13, 14]. Hydrogels materials are three-dimensional network structures build up from physically or chemically crosslinked polymers. Several researches [13, 15] claimed hydrogels are materials with excellent water absorption and desorption performance with high water evaporation rate. Moreover, the hydrogels can be designed to be responsive to external stimuli [11, 16], such as magnetic fields, electric fields temperature changes and more. Furthermore, hydrogels are low cost materials and environmental friendly [17]. The mentioned advantages ensure hydrogels can be promising candidate for the drying of biobased materials and the substitution of conventional hot-air dryers. For the application of hydrogels in biobased materials dehydration process, the understanding of synthetic routes and the swelling mechanism are indispensable. Electro-responsive hydrogels, synthesised through free radical polymerisation [18, 19], are generally copolymerization [18, 19] of an ionic monomer and a non-ionic hydrophilic monomer. Luo et al. [19] reported the use of ionic monomer 2-acrylamido-2-methyl-1-propanesulfonic acid (AMPS) blended with acrylamide (AM) to analyse the mechanism swelling and deswelling behaviours of the hydrogels. The molar ratio between the monomers [19] influences the swelling ratio, the water exudation amount and the charge density of the hydrogels.

The characterisation of the hydrogels [19], there is scanning electron microscope (SEM) for the morphology structure at dry and swollen state, and Fourier transform infrared spectroscopy (FITR) for the chemical structure, the swelling ratio for the amount of water uptake, tensile test for the mechanical properties. However, there is a lacks of methods for the charge density distribution visualisation. Nevertheless, there are researches [15, 20] over the application of fluorescence microscopy, and thus the confocal laser scanning microscopy (CLSM) to achieve three-dimensional restructuring and super-resolved images regarding the microstructure [15] and topology [20] of hydrogels. The principle of fluorescence microscopy [21] to examine fluorescent substances in a microscope. The technique offers high sensitivity and specificity. One of the applied fluorescent dyes is Rhodamine B [22], whose fluorescence excites with colour red is extremely photostable and has a high quantum yield. Moreover, Rhodamine B molecule is positively charged, and according to the electrostatic attraction, the application of Rhodamine B to trace the negatively charged polymer chains. Subsequently, the visualisation of the charge density distribution in the hydrogels will be feasible. Therefore, the goal of the research is to prove the concept of using Rhodamine

B fluorescent dye to visualise the charges distribution through the variation of molar ratio of the monomers in the synthesised random copolymer hydrogels.

The research question is: To what extent is the visualisation of electric charge density in the random copolymer hydrogels feasible under a confocal laser scanning microscopy with the use of Rhodamine B?

The secondary questions is: How does the monomers molar ratio influence the distribution of electric charge density in the hydrogels?

In this paper, a comprehensive theory was given in Chapter 2; followed by a detailed experimental set-up and planning in Chapter 3, where a series of poly(hydroxyethyl methacrylate) (PHEMA)-*ran*-poly(3-sulfopropyl methacrylate potassium salt) (PSPMA) had been synthesised by free radical polymerisation in nitrogen environment. The hydrogels samples were characterised with swelling ratio, optical microscope, scanning electron microscope, Fourier transform infrared spectroscopy, and confocal laser scanning microscopy. The results were discussed in Chapter 4, and concluded in Chapter 5. For supplementary information, an Chapter 6 was provided.

2 Theory

The word *hydrogels* appeared for the first time in literature in 1894 [12], in which the material was described to be colloidal gel made with inorganic salt [12, 23]. Hydrogels are characteristic for the high water affinity [23], soft and stretching material character, which result in swelling behaviours. The development of hydrogels that matches with nowadays description started in 1960, when the first synthetic hydrogels were synthesised using poly(2-hydroxyethyl methacrylate) (pHEMA) [12, 23]. The focus then was making a wide trial of crosslinking procedures and attempts to alter the monomer or polymer compositions using an initiator. Additionally, the material development focused on high swelling and good mechanical properties [12]. At the start of the seventies, *smart hydrogels* was an emerging concept [12, 23], which referred to materials that are responsive to external stimuli such as an electric field, pH or temperature [11, 10]. Recently, the applications of the hydrogels [23] focus on, for instance, separation technology, agriculture and horticulture, or wastewater treatment. Among these applications, hydrogels are characterised by good swelling capacity of (contaminated) solutions or water.

The capability of hydrogels to absorb a considerable amount of water is due to the peculiar three-dimensional crosslinked structure, whereby the hydrogels are able to maintain the structure at swollen state [10, 12, 23]. The responsible interactions [10, 12] for the water sorption phenomenon at the swollen state is the counterbalance of capillary, hydration and osmotic forces, and the resistance force of the crosslinked polymer chains.

2.1 Classification of hydrogels

There are several classifications of hydrogels[10, 16] based on parameters such as the source of materials, the polymeric composition, the ion charge and the crosslinking types.

2.1.1 Source of materials

The source of materials refer to the distinction between natural and synthetic hydrogels [10, 11, 16]. Natural hydrogels[10], for example, polysaccharides, are characterised by non-toxicity and low price. However, natural hydrogels are generally more delicate, and hence they possess poor mechanical properties. Synthetic hydrogels [12], on the other hand, take precedence over the natural hydrogels due to a facile synthesis protocol with tailored-made properties and cost effectiveness. Consequently, the synthetic hydrogels provide flexibility to tune the mechanical properties according to the application [10]. Synthetic hydrogels are synthesised via chemical polymerisation with the use of manufactured monomers [23], the resulting hydrogels can be homopolymeric, copolymeric and multipolymeric.

2.1.2 Polymeric composition

The classifications based on the polymeric composition [10, 16, 23] are homopolymer, copolymer, multipolymer and interpenetrating network (IPN). Homopolymer hydrogels are polymer chains derived from one single species of monomer, in which the structural framework depends on the polymerisation techniques, used crosslinker and the nature of the monomer[23]. Copolymer hydrogels [10, 23] contain two or more monomer species where one of the monomer is hydrophilic and responsible for the swelling. Copolymer hydrogels are synthesised via chemically crosslinking both of the monomers with the use of an initiator and a crosslinker; or physically crosslinked [23] by forces from chain aggregation, hydrogen bonding, ionic interactions and ion-polymer complexations.

2.1.3 Crosslinking configurations

Based on the crosslinking, the hydrogels can be arranged into different configuration types, such as graft, random, block and alternate. Multipolymer hydrogels [23], similar to copolymer hydrogels, are produced via polymerising or corsslinking from three or more polymers. IPN [10, 23], are

hydrogels derived from two independent type of polymer chain crosslinked with each other without any chemical bond. The first polymer network is linear, and it diffused into the second polymer network which has a crosslinked network.

The type of crosslinking indicates the junction between the macromolecules. Depending on the crosslinking methods, hydrogels can be classified into chemically crosslinked by covalent bonds or physically crosslinked by non-covalent interactions [10, 16]. As for chemically crosslinked hydrogels, the polymer chains are linked by chemical bonds under the action of a crosslinker, light or high-energy radiation [23]. Subsequently, the covalent bond provides mechanic rigidity to the network structure. Physically crosslinked hydrogels, on the other hand, are formed through interactions such as hydrogen bonding, hydrophobic interaction, polymer chain entanglement. According to the type of crosslinking, there are corresponding polymerisation routes. There are seven examples listed in Table 1. The different preparation methods result in three classes of hydrogels [10, 16]: homopolymers, copolymers and interpenetrating networks (IPN).

2.1.4 Electric charges

The nature of electric charges on the crosslinked chains is classified into three type of hydrogels [10, 16, 23]: neutral, ionic and ampholytic. Neutral hydrogels [23], are the ones with no charge on the backbone or side group. Ionic hydrogels [10, 23] can be cationic or anionic, depending on the charged group. The ionic hydrogels have ionic groups attached on the polymer chains backbone that ionise in a certain pH to develop fixed charges. For this reason. ionic hydrogels are responsive to the change of pH, and thus the swelling ratio behaves differently. The classification of pH-sensitive hydrogels is dependent on the ionic group, and it can be anionic or cationic. Anionic hydrogels have acidic pendant groups (i.e. carboxylic or sulphonic acid) on the polymer backbone. These hydrogels swell better in high pH due to large osmotic swelling force induced by the ionisation of the acidic pedant groups [23, 24]. For cationic hydrogels, the swelling is better in low pH. Ampholytic hydrogels [23, 24] carry both positive and negative charge on the same polymer chains, the balance of the charges leading to a no net electric charges on the polymer backbone.

There are seven polymerisation method mentioned in Table 1, whereby free radical polymerisation (FRP) [18, 25] is widely used to synthesise chemically crosslinked, high molecular-weight polymers from a variety of monomers. Moreover, free radical polymerisation can polymerised or copolymerized nearly all the alkenes [26], and it is the key synthesis route to obtain (co)polymers and composites [25, 27].

Table 1: Type of polymerisation mechanism

Crosslinking	Type of polymerisation mechanism			
Chemical	Free radical polymerisation	Radiation	Crosslinking of water-soluble polymers	
Physical	Ionic bonding	Crystal crosslinking	Hydrophobic association	Hydrogen bonding

2.2 Free radical polymerisation mechanism

The general reaction mechanism of FRP [25, 26, 28, 29] is in the following order: initiation, propagation and termination.

Radicals [29] are species with an unpaired electron, these electrons are used to trigger the initiation of free radical polymerisation. There are several options to generate radicals [25, 26], for example, temperature, photolysis, ionization irradiation, redox reaction, plasma, sonication. Radical initiation works the best on the vinyl group of the monomer, whereby acrylates and the methacrylates are the most common monomers used in FPR [25, 26]. The choice of monomers are generally small water-soluble molecules with a double bond [10, 11, 17].

The initiation consists of two steps. The first step is the homolytic cleavage the bond of the initiators to create radicals. At the second step, the radicals are transferred from the initiators to the monomer by cleaving the carbon-carbon double bond. [25, 29]. There are several initiators available for FRP, some examples of initiators [10, 11] are potassium

persulfate (KPS), ammonium persulfate (APS), ceric ammonium nitrate, 2-2'-azobisisobutyronitrile (AIBN) and N, N, N', N'-tetramethylethylenediamine (TEMED). The crosslinkers used for the radical polymerization [11] are N, N'-methylenebisacrylamide (MBA), ethyleneglycol dimethacrylate (EDGMA), melamine trimethyllacrylamide and melamine triacrylamine [12].

The polymer chains propagate after the formation of radicals, whereby the loose electron will attack the unsaturated monomer. In the vinyl group of the unsaturated monomer, there is a σ bond and a π bond. The electrons between the π bond is more loose in comparison to the σ bond, hence the free radical uses the electron from the π bond to form a more stable bond with the carbon atom. At meanwhile the other electron returns to the second carbon atom and turn whole molecule into a another radical [25, 29]. This step proceed consecutively to extend the chain growth.

Termination is the step at which the radical at the end of the polymer chains couple together to form one long chain [25, 26]. With the variation of the initiator concentration, the polymer chains will result different. For instance, the initiator concentration should be kept low if longer chains are desired.

Copolymerization [30, 31] is the product of the polymerisation of two or more monomer type units, whereby results in the formation of polymer chains. There are four main categories which further deepen into the classification of the copolymers produced from bifunctional monomer[25, 30, 32].

1. Statistical or random copolymers involve a random distribution of the two monomers along the copolymer backbone. The distribution is determined by the reactivities of the individual monomers. The nomenclature for this copolymer type is poly(A-*ran*-B).
2. Alternating copolymers have a regular alternation of the two monomers throughout the copolymer backbone. The nomenclature is denoted as poly(A-*alt*-B).
3. Block copolymers have substantial arrangement of blocks or sequences of each monomer in the copolymer backbone. The nomenclature is poly(A-*block*-B).
4. Graft copolymers, poly(A-*graft*-B), are the ones that the blocks are grafted as branches onto the backbone of other monomer.

Random or alternating copolymers are traditionally synthesised by free radical, anionic and cationic techniques [32]. In order to improve the control of the microstrcutre of the macromolecules, controlled/living radical polymerisation (CRP) was introduced to the synthesis of copolymers. Some examples of CRP [32] are nitroxide-mediated polymerisation (NMP), atom transfer radical polymerisation (ATRP) and reversible addition fragmentation transfer (RAFT). It had been reported that random copolymers were synthesised with RAFT or ATRP, and alternating copolymers with NMP. Block and graft copolymers were synthesised by NMP, ATRP and RAFT [32].

In addition to the arrangement of the distribution of the monomer, copolymers are also described according to the existence or arrangement of the branches in the polymer chains [25]. Linear copolymers are the ones with a single main chain, for instance, gradient copolymers are the monomer compositions gradually changes along the polymer chain. Other specific copolymers such as star, brush and comb. At the present synthetic polymeric materials, there are three categories for the polymers: linear, branched, and crosslinked.

2.3 Smart Hydrogels

As mentioned, synthetic hydrogels open possibilities to tailor the properties of the materials according to the applications. The materials with the abilities to respond to an external stimuli are considered as smart hydrogels [33, 34]. Smart hydrogels can further classified as physical or chemical stimuli responsive hydrogels [34]. Physical stimuli include temperature, electric or magnetic fields and mechanical stress [23]. Chemical stimuli include pH, ionic factors and chemical agents [23]. For the project, the focus in on the hydrogels that are able to respond to an electric field. The hydrogels that are sensitive to an electric field have a large amount of ionisable groups in the polymer chains, and they are commonly known as polyelectrolytes [33, 34]. In an electric field, the

mobile ions inside the hydrogels is regulated. Hence the hydrogels experience shrinkage or swelling under the influence of an electric field [33, 34].

2.4 Characterisation techniques

For the characterisation of the hydrogels, there are several methods mentioned in the literature. The common techniques include the swelling ratio to determine the water uptake behaviour, scanning electron microscope (SEM) to observe the surface and structure of the pores, optical microscope for quick check about the material structure, Fourier-transform infrared spectroscopy (FTIR) for the chemical composition of the material [35, 36]. For the project, confocal laser scanning microscope (CLSM) is applied to observe the electric charges density inside the hydrogels. The mechanism of these techniques are briefly described as follows.

2.4.1 Swelling behaviour

Hydrogels are able to expand the volume and the size to contain large amounts of water, and the process of water uptake is called swelling. The swelling behaviour of the hydrogels depends on some characteristics of the material [10, 37], such as the mechanical properties, the degree of crosslinking, the degradation rate in the solvent, the extend of porosity and the structure of the pores.

In the relation to the pore sizes [37], there are four categories: non-porous, micro-porous, macro-porous and super-porous. Each category has the corresponding morphology, external stimulus, swelling mechanism and the swelling rate. The morphology of the different categories results in various pore sizes. Non-porous contain only small pores without network porosity. Micro-porous size ranges from 10nm to 100nm. Macro-porous ranges from 0.1μm to 1μm. Super-porous are the pores with size above 10μm. Based on the swelling experimental results, the swelling ratio at the equilibrium state is calculated by the following equation [10, 35, 38].

$$Swelling(g/g) = \frac{W_s - W_d}{W_d} \qquad \text{(eq. 1)}$$

Here, W_s is the swollen hydrogels weight, and W_d is the dry hydrogels weight. The unit for the weights is in grams.

2.4.2 Fourier-transform infrared spectroscopy (FTIR)

Infrared (IR) spectroscopy [35, 39] is a cost-effective and reliable technique to identify the chemical structure of both organic and inorganic compounds. Furthermore, IR allows the possibility of analysing substances at different states, such as liquid, solid and gases.

Fourier-transform infrared spectroscopy (FTIR) [39] is the most significant advancement in IR. FTIR generate considerate improvement at minimising spectral acquisition time while maintaining the quality of the spectra. The basic principle of FTIR is to subject the substance in an electromagnetic radiation in the IR region of the spectrum, whereby the components of the substance (i.e. chemical bonds) can be excited or absorb the infrared light at specific frequencies or wavenumber [40]. The resulting IR absorption spectra is a fingerprint characteristic of the measured sample. On the spectra, different absorption patterns could vary from broad to sharp depending on the chemical bonds.

2.4.3 Optical Microscope

Optical microscopy, or light microscopy [40, 41], is one of the first instruments used to study surface topology. The fundamental components of the optical microscope [42] are the objective lens, an ocular and a light source. The system of optical microscope uses visible light and lenses to magnify the images of a (small) sample [41]. The resolution of an optical microscope is determined by its 1) optical components, especially the objective and its numerical aperture (NA), and 2) wavelength of light [43]. NA is related to the refractive index (n) of a medium when a light passes through, and the

angular aperture (α) of a specific objective. The mathematical expression for the NA is described as (eq. 2), where the resolution is better than a higher NA value[43, 44]. For the light wavelength, shorter wavelengths result in better resolution and are capable of resolving greater details than long wavelengths.

$$NA = n \sin \alpha \quad \text{(eq. 2)}$$

The lateral resolution of the image can be described with the Rayleigh criterion. Here 1.22 is a constant, λ is the wavelength of the light shone on the specimen. To acquire a well resolved image, the working distance is the key parameter. The working distance is the distance between the objective and the specimen in focus, and each objective was designed with a numerical aperture that resolve and magnify an image under a certain working distance. The resolution and magnification depend on the numerical aperture of the objective, and the magnification ranges from 5x to 100x [42].

Optical microscope allow a direct observation of the specimen by eye, and generate images revealing the material structure in different a resolution range from 0.2 to 0.5μm [41, 45]. Even though hydrogels image acquisition is viable using optical microscope, the resolution is limited for think samples [45], and it is difficult to resolve images at a nanometre scale [40].

$$r = 1.22 \frac{\lambda}{NA} \quad \text{(eq. 3)}$$

2.4.4 Scanning Electron Microscope (SEM)

The invention of SEM was first built in 1942 with a resolution of 50nm and magnification of 8000x [46]. SEM is a technique to analyse the material surface in a vacuum, and the principle is to scan the sample surface with a focused beam of electrons [40, 41]. The interactions between the electron and the atoms in the material generates an emission of electrons and photons. The emitted electron and photons are collected and located with the detector to produce an image, and the image contains information regarding the surface topology of the sample. The resolution of SEM can achieve better than 1nm [41, 46].

Furthermore, SEM-energy-dispersive X-ray spectroscopy (EDX) [41] provides elemental or chemical analysis of the sample. The principle is to investigate the interaction between the X-ray excitation source and the sample since each element has a unique atomic structure and hence a unique set of peaks in the X-ray spectrum.

2.4.5 Confocal Laser Scanning Microscope (CLSM)

Confocal laser scanning microscope (CLSM) [47, 48] is one of the most important advanced in the field of fluorescence imaging. In comparison to the electron microscopy (i.e. SEM), CLSM has to trade-off between the image resolution and the light collection efficiency. Nevertheless, CLSM requires considerably less amount of specimen, and allows a reconstruction of three-dimensional (3D) or more dimensional live imaging. The word *confocal* means the image was obtained from only one focal plane, rejecting the signals from above or below targeted focal plane. This is accomplished with a focused *scanning laser beam*, which the image was acquired point by point under a localised laser excitation.

The principle of CLSM [47] is to analyse the fluorescence emitted by a fluorophore molecule after being irradiated by a laser beam. Each fluorophores has its two characteristics spectra [47], an excitation spectrum and an emission spectrum. The excitation spectra corresponds to the wavelength that excite the fluorophores; whereas the emission spectrum is a reflection of the excited spectrum, but shifted to higher wavelengths. The sample preparation for CLSM is to immerse the hydrogels in a aqueous solution of fluorescent dye for 24 hours [20]. Fluorescent dye examples are, for instance, fluorescein isothiocyanate or rhodamine B isothiocyanate [20]. To remove the excess of

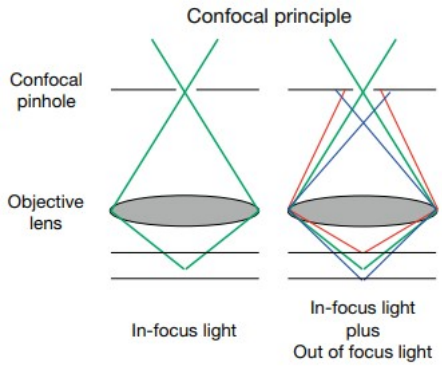

Figure 1: The principle of a confocal microscope. The image is acquired only from the focal plane, the out-of-focus plane light is rejected. Figure taken from [48]

fluorescent dye, the samples are rinsed multiple time with water. Afterwards, the samples are stored in the dark to prevent photobleaching and keep fluorescent active.

The fundamental piece of a CLSM is the *pinhole* [47, 48], which filters spatial fluorescence and eliminates out-of-focus light which subsequently minimises the optical noises result in sharp fluorescence imaging. The diameter of the pinhole is described as an Airy unit (AU), and the default setting for the pinhole is $1AU$ [47, 49]. At the image plane, an AU is defined as the zeroth order potion of the central diffraction spot [50]. In practice, the pinhole is not recommended set to be lower than 0.7AU [49].

The image acquisition of CLSM is through the scanning galvanometer mirrors in which the laser beam swept incrementally over the entire sample in x and y direction to produce an image of optical section [50]. The collection of optical section from bottom to top of the sample is called *z-stack* [49, 50], and each new section the focal points changes; hence the output is a series (stack) of two-dimensional (2D) images. With the series of stacks, a three-dimensional (3D) image of the sample can be reconstructed. For the CLSM image analysis, Matlab or ImageJ and ImageJ variant Fiji (Fiji Is Just ImageJ) [47, 51] are widely used.

2.4.6 Fiji - ImageJ

ImageJ and its variant Fiji are the most widely used for image analysis [51]. Fiji is incorporated with numerous plugins and additional documentation. For example, Fiji is capable of reading and displaying the image formats and metadata. Metadata [51] includes relevant information of the acquired image, such as the size of pixel, time of exposure, details of fluorescence channel, or used objective lens. Furthermore, the z-stacks are treated as a series of images whereby it is very convenient for 3D rendering and analysis.

3 Materials and Methods

This chapter describes the experimental methodology which comprises the materials, the synthetic procedure, the characterisation techniques and the data processing.

3.1 Materials

2-(Hydroxyethyl)methacrylate (HEMA, 97%, CAS 868-77-9), 3-sulfopropyl methacrylate potassium salt (SPMA, 98%, CAS 31098-21-2), ammonium persulfate (APS, 98%, CAS 7727-54-0), $N, N, N'N'$-tetramethylethylenediamine (TEMED, 99.5%, CAS 110-18-9), N, N'-methylenenbisacrylamide (MBA, 99%, CAS 110-26-9), ethylene glycol (EG, 99.8%, CAS 107-21-1), Rhodamine B as fluorescence dye $\geq$95% were purchased from Sigma Aldrich. Activated basic alumina was used to adsorb the inhibitors in HEMA, and the purified HEMA was stored at room temperature.

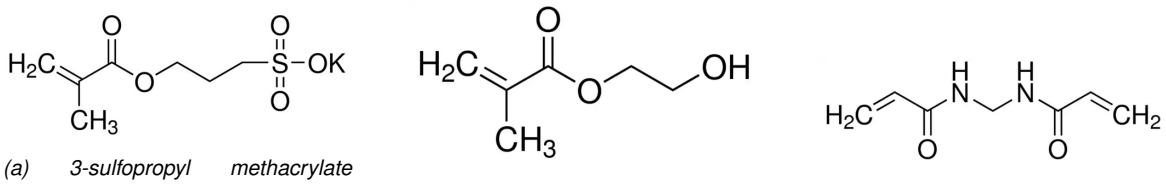

(a) 3-sulfopropyl methacrylate potassium salt *(b) 2-(Hydroxyethyl)methacrylate* *(c) N, N'-methylenenbisacrylamide*

Figure 2: Molecular structure of the monomers (SPMA&HEMA) and the crosslinker (MBA)

3.2 Synthetic procedures

The hydrogels were prepared by free-radical polymerisation of certain amounts HEMA, SPMA, MBA, APS and TEMED dissolved in 1.0mL Milli-Q water under purging with nitrogen gas. To ensure the solid chemicals were completely dissolved in the solvent before the polymerisation, the chemicals were mixed, stirred and purged in two separate 5.0mL large vials. In profile A, SPMA and TEMED were dissolved in 0.4mL of water, In profile B, APS and TEMED were dissolved in 0.6mL of water. Both solutions were stirred until everything was dissolved, followed by purging for 5 minutes. Afterwards, the solution were mixed and with the use of a syringe, the mixed solution was transferred into 3 straws of 5cm to obtain hydrogels in cylinder geometry. The polymerisation reaction was carried out at room temperature for 4 hours. After the hydrogels were cut into 3.0mm thick disks. The products were soaked in Milli-Q water for 24 hours to remove any residue chemicals. For the characterisation of the hydrogels, the products were first frozen with liquid nitrogen, and then freeze-dried at -50℃ for 24 hours. This report recorded 5 series of molar ratio between HEMA and SPMA, and each molar ratio synthesis was repeated twice. The material amount was shown in the Table 2.

Table 2: Hydrogels synthesised by different monomer molar ratio combinations. The amount of APS, TEMED and MBA were kept constant throughout out the synthesis series. The total volume of water is 1.0mL.

Materials	SPMA molar composition				
	100%	75%	50%	25%	0%
SPMA (g)	0.492	0.369	0.246	0.123	0
HEMA (mL)	0	0.072	0.143	0.021	0.287
APS (g)	0.0091				
TEMED (μL)	0.99				
MBA(g)	0.0062				

3.3 Characterisation of hydrogels

The chemical composition of the freeze-dried hydrogels were tested by FTIR using Bruker Alpha with the wavenumber range from 4000cm^{-1} to 400cm^{-1} at room temperature. Surface morphology were examined by optical microscope using Olympus BX60, and SEM using Jeol7610-Plus. The charge density distribution and the 3D reconstruction of the hydrogels were obtained by CLSM using Zeiss LSM880. The images were obtained from the Zeiss LSM880 computer software *ZEN*.

To determine the swelling ratio (SR), the freeze-dried hydrogels were weighed at dry state, and after keeping the hydrogels in distilled water for 24 hours. Swelling ratio (g/g) was calculated with the equation 1: Here, W_s is the swollen hydrogels weight, and W_d is the dry hydrogels weight. The hydrogels were weighed in grams.

3.4 Characterisation of permanent charge density using CLSM

To use the CLSM for the observation of the electric charge density distribution within the hydrogels, a 0.1M stock solution of Rhodamine B was prepared. In order to find the most suitable concentration, the stock solution was diluted to 1.0mM and 0.1mM. In the literature, 0.1mM yields the best condition for imaging using confocal microscopy [52]. The freeze-dried hydrogels were placed in the respective solution, and kept for 24-48 hours. To ensure the fluorescence dye bond with the charged polymer chains, the dyed hydrogels were washed to remove the excess of fluorescent dye in Milli-Q water until the water was transparent.

3.5 Data processing

The goal of the project is to prove the concept of using CLSM to observe the electric charge density distribution within the hydrogels, which is the reason Rhodamine B was used. The images acquired from SEM can indicate the pore sizes and the morphology of the hydrogels. However, due to lack of literature regarding the copolymerization of SPMA and HEMA, it is not possible to have a direct comparison of the pore sizes. Therefore, the SEM images for this report were qualitative data rather than quantitative.

FTIR was used to compare the chemical composition between different monomer molar ratios, and the bonding stretching of different functional groups. For the comparison, the absorbance data points of all the samples were plotted in Origin-2019b. Since the plots were from different samples, the data points were normalised. Comparing the molecular structure of SPMA and HEMA, both molecules have a ester carboxyl group. For this reason, the data points would be normalised at the characteristic signal range of ester carboxyl from 1750cm^{-1} to 1730cm^{-1} in reference of 100% molar% SPMA hydrogels.

The swelling ratio of the hydrogels, on the other hand, provide a quantitative number regarding the uptake water amount. However, there is limited literature describing the swelling behaviour of SPMA-HEMA copolymer hydrogels. Therefore, error analysis of the experimental data set would prove the reliability and credibility of the data. The error propagation of the data was analysed in the following manner:

1. Calculate the mean weight value of the dry and the swollen hydrogels from each SPMA molar%.
2. Calculate the swelling ratio using equation 1.
3. Calculate the mean value of the swelling ratio, Q represents swelling ratio.

$$Q = \overline{Q}_i = \frac{1}{n}\sum_{i-1}^{n} Q_i \qquad \text{(eq. 4)}$$

4. Determine the standard deviation of the dry and swollen hydrogels.

$$s = \sqrt{\frac{1}{n-1}\sum_{i=1}^{n}(m_i - m)^2} \qquad \text{(eq. 5)}$$

5. Calculate the error for swelling ratio.
6. Calculate the 95% CI with the calculated standard error.

4 Results and Discussion

In this chapter, the samples synthesised according to Table 2 were analysed and characterised with the techniques described in chapter 3. The discussion of the results were based on the observations and supported by current available literature researches.

4.1 Synthesis of hydrogels

For the synthesis of hydrogels, with the only exception of the 0% SPMA composition, the rest SPMA composition end products were transparent, flexible and able to absorb considerable amount of water. Images can be found at Appendix section 6.1. Some explanations for the non-transparency and low swelling could be the structure of the material, the effect of the crosslinkers content, the quantity of hydrophilic moieties, the solubility in water or the size of the pores. In the literature, p(HEMA) is widely considered to have low swelling ratio [7, 53], this is due to the fact that HEMA is less soluble in water [53]. Copolymerization of HEMA with an hydrophilic monomer would increase the swelling property of the hydrogels [53]. However, the addition of another monomer would alternate the structural heterogeneity in the end product. The effect of the pore sizes could be further verified with SEM and CLSM imaging. To solve the problem of non-transparency, because CLSM works $only$ with transparent hydrogels, different synthesis methods [36, 54] from the literature were taken into consideration, which results in several protocols with small modifications. Considering the amount of crosslinker would affect the swelling and the structure of the hydrogels, the second synthesis of 0% SPMA composition hydrogels were synthesised with 0.062mg of MBA, which was 10 magnitude lower than the original protocol listed in Table 2. Nevertheless, the end products presented similar characteristics as the first synthesised 0% SPMA hydrogels. For more information regarding the synthesis of transparent 0% SPMA see Appendix 6.2.

The protocol for the transparent hydrogels synthesis kept the same amount of chemicals as listed in Table 2 for 0% SPMA composition, and with the addition of 1.0mL ethylene glycol to enhance the solubility of HEMA. The swelling ratio for the trials were recorded, since the irrelevance to the report the data were included in Appendix section 6.2.

4.2 Swelling behaviour

After synthesising hydrogels with different SPMA/HEMA monomer ratio as stated in chapter 3, the swelling behaviour of the products were measured and the averaged swelling ratio were summarised in Table 3.

Table 3: The average swelling ratio under different SPMA composition and the respective statistical errors

SPMA composition (%)	**Averaged swelling ratio (g/g)**	**Error bar averaged swelling ratio (g/g)**	**95%CI (g/g)**
100	119.9281	6.2614	5.2355
75	63.8983	4.1872	4.3949
50	52.9781	5.94187	7.3766
30	56.6286	5.8622	14.5637
25	143.8925	13.04004	10.9035
20	66.4661	7.22496	17.9493
0	2.6128	0.11316	0.2811

The presented results in Table 3 showed the synthesised hydrogels with 100%, 75%, 50%, and 25% molar ratio of SPMA monomer absorbed considerable amount of water. Whereas, the 0% SPMA (100% HEMA) molar ratio hydrogels had a white colour and were only able to swell roughly 2% from its dry state.

The anionic group (SO_3^-) present in the SPMA monomer is a hydrophilic moiety, whereby it is logical to observe an increasing trend as the SPMA composition increases in the polymer chains. The results of 0%, 50%, 75% and 100% SPMA composition followed the expected increasing trend, whereas the 25% SPMA composition had a exceptionally high swelling ratio with 127.9044 g/g. In order to verify whether this data point was an outlier, 2 additional synthesis with 20% and 30% SPMA composition were performed. The averaged swelling ratio were 66.4661 g/g and 56.6286 g/g respectively.

In addition to the change of colour, the rigidity of the hydrogels decreases from higher SPMA composition to the lower SPMA composition. The hydrogels with 100% SPMA composition were stronger, and the hydrogels were able to maintain its shape upon being pulled out of the straw. Similarly, the hydrogels of 0% SPMA composition were able to maintain the shape, but they were softer. The hydrogels synthesised with other compositions had the similar texture and fragmentation while being pulled out of the straws.

After the measurement of the swelling ratio, the data were presented in Figure 3. There is an evident trend that the water uptake decreases in function of the SPMA composition, this is due to the reduction of hydrophilic moieties SO_3^- from SPMA present in the polymer chains. Moreover, HEMA molar percentage increased as SPMA molar percentage decreased. The hydroxyl groups $-OH$ from HEMA form intermolecular or intramolecular hydrogen bonds in the polymer chains [36, 55]. The bonding between $C = O$ and $O - H$ would prevent the polymer chains making hydrogen bond with the water, and hence lowered the swelling ratio [36]. However, there was an exception at 25% SPMA composition, with a swelling ratio of 127.9044 g/g, which is larger than 100% SPMA composition. An explanation could be the combination of this molar ratio yielded a different structure such that the pore sizes were larger. This assumption could be verified with SEM imaging. At comparing the error bars of these compositions, the swelling ratio at equilibrium state for both 25% and 100% compositions were very close. In fact, there was no clear trend in the graph 3, but there were two peaks from 25% and 100% SPMA composition. This observation differs from the literature copolymerization of p(HEMA) with another monomer. For instance, Hernández et al [56] presented HEMA copolymerized with N,N-dimethylacrylamide (DMAa; 99%), and the swelling behaviour at equilibrium of the hydrogels showed a linear trend. There were researches [36, 57] presented swelling behaviour at equilibrium as an exponential function. The different swelling behaviour is due to the change in different parameters. Hernández et al [56] synthesised hydrogels under free radical polymerisation with the use of AIBN as an initiator. Liu et al [36] chose have a controlled radical polymerisation and synthesised hydrogels at 60℃ for 24 hours.

The error bars and the 95% CI values were relatively low, which showed the reliability of the data points. The 95%CI for the 20% and 30% SPMA composition data points were slightly higher because the synthesis was only performed once.

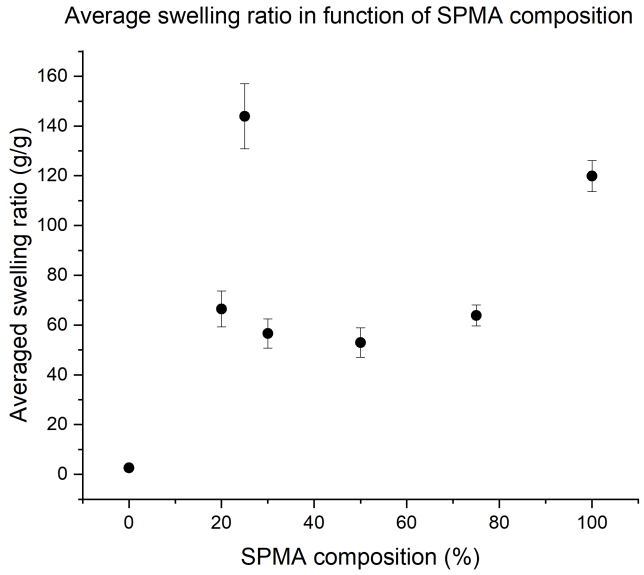

Figure 3: The average swelling ratio in different SPMA molar% composition. 25% SPMA and 100% had the highest swelling. The error bar was derived form the standard deviation of each sample set

4.3 Optical microscope imaging

The freeze-dried hydrogels were glassy, white and fragile, except for the 0% SPMA composition for being only brittle and non-transparent, these material properties allowed the peeling of thin hydrogels slices for the morphology imaging.

The overview of the hydrogels was taken with a magnification of 5x, the material had a nest-like structure. For 100% SPMA composition, some bubbles were observed in different magnification, and they were assumed to be water bubbles. To verify the assumption the 100% composition samples were further dry in a vacuum oven, and the samples before and after oven-drying were compared by using optical microscope and FTIR. Evidently, the hydrogels after oven-drying showed less bubbles. This means hydrogels of 100% SPMA composition were had a very high affinity to water, and the actual swelling ratio could be larger than the measured value.

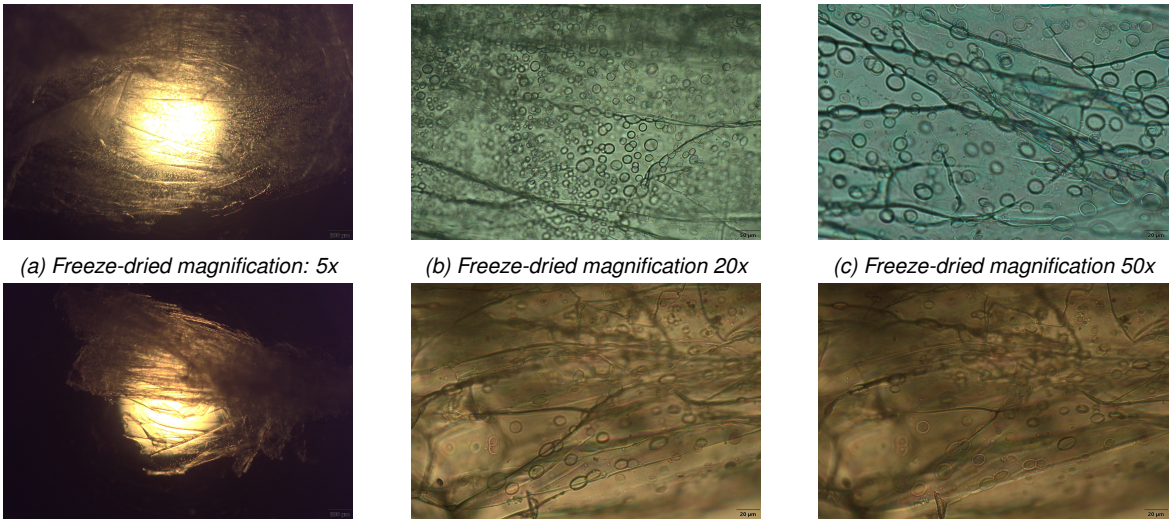

(a) Freeze-dried magnification: 5x *(b) Freeze-dried magnification 20x* *(c) Freeze-dried magnification 50x*

(d) Oven-dried magnification: 5x *(e) Oven-dried magnification 50x* *(f) Oven-dried magnification 50x*

Figure 4: Comparison between freeze-dried 100% molar% SPMA a) to c), and oven-dried d) to f) 100% SPMA composition hydrogels under different magnifications

For the rest of the samples, trends and more translucent parts were observe, and these were expected to be the polymer chains and the pores. However, the optical microscope had the limitations of sample thickness and observation of the surface morphology differences. SEM and CLSM would implement the understanding and visualisation of the surface morphology.

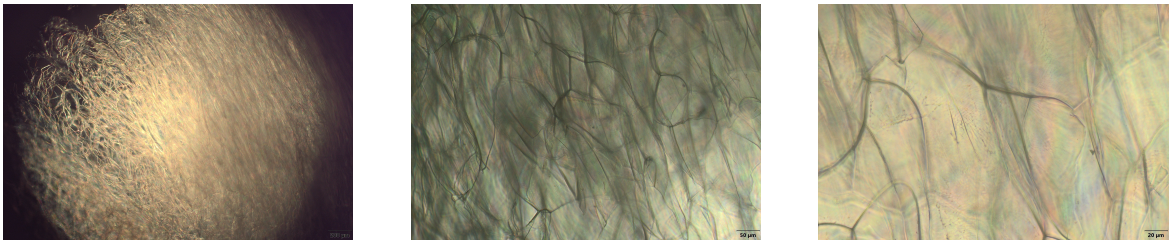

(a) Magnification: 5x *(b) Magnification 20x* *(c) Magnification 50x*

Figure 5: 25% SPMA composition under different magnifications

4.4 Fourier-transform Infrared Spectroscopy (FTIR)

The FTIR allowed the understanding of the chemical composition of the hydrogels, and the interpretation of the signals would indicate the interaction between molecular bonds. In order to have a comparison between spectra, because the absorbance differed per SPMA composition percentage, the spectra were normalised at the reference of 100% SPMA composition. The normalisation required a common signal that was present among the spectra; a signal around 1717cm^{-1} appeared at every spectra, and this is a characteristic wavenumber for the ester carboxyl $C = O$ group stretching [58]. Moreover, the ester group is present in both SPMA and HEMA, therefore it was a reasonable peak for normalisation.

Figure 6 comprised the normalised FTIR spectra of the different SPMA composition percentages. There were signals around 3500cm^{-1} representing presence the stretch of a hydroxyl ($-OH$) groups, the broad signals indicate intermolecular hydrogen bond that could be the interaction between the hydroxyl groups or the bonding with water [59]. In the Figure 8e the 100% SPMA composition had the largest signal even though the molecule does not have hydroxyl group. This mean the high water affinity was originated from the interaction between the hydrophilic moiety SO_3^- and the water. For this reason, the spectra which had SPMA in its composition were slightly shifted to

at 3451cm^{-1} in comparison to 0% SPMA at 3350cm^{-1}. The difference at the wavenumber was due to the presence of hydroxyl group in 0% SPMA (100% HEMA), consequently, the water interacts with the hydroxyl group. Furthermore, there was a trend that the peak were shifting from 3451^{-1}cm to 3350^{-1}cm and the absorbance lowered at decreasing SPMA molar% in the hydrogels composition. The FTIR spectra from Hernández et al [56] showed a similar trend, a vibration of the hydroxyl group was detected at 3390cm^{-1}, and the signal gradually shifted to 3450cm^{-1} at an increasing composition of DMAa monomer.

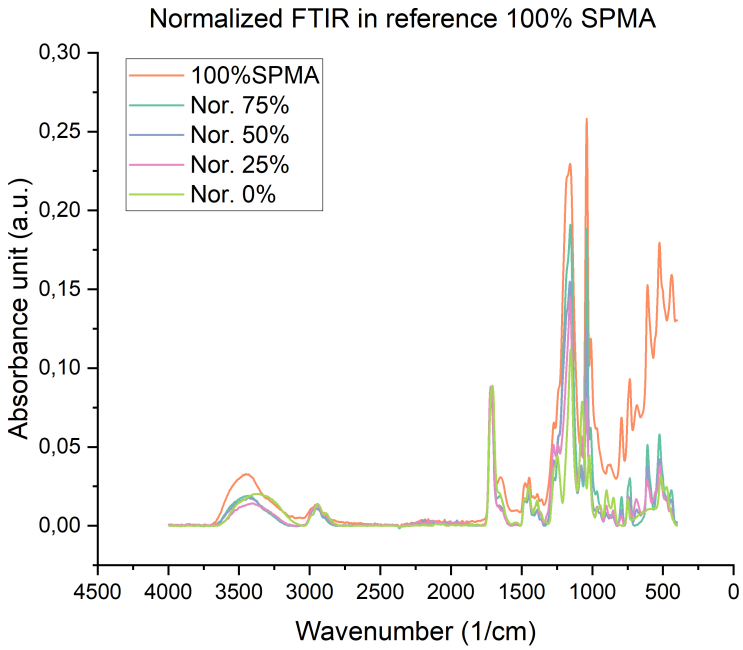

Figure 6: Normalised FTIR with reference of 100%SPMA at the peak of C=O

At the range from 2950cm^{-1} to 3000cm^{-1}, and the range from 1400cm^{-1} to 1500cm^{-1} there were signals of roughly the same intensity. It was difficult to assign these signals to a particular functional group of the hydrogels. The MBA molecule has functional groups that can be classified as secondary amines, carboxyl of secondary amides or ketones, The characteristics wavenumber for secondary amines is at the range 3350cm^{-1} to 3310cm^{-1}, and for carboxyl of secondary amides would be a strong signal at 1680cm^{-1}. However, these signals were not evident in the FTIR spectrum. According to the Table 2, the molar amount of crosslinker with respect to the monomers is 1.702% whereby the low value could explain the signals were possibly overlapped by other signals in the FTIR spectrum. Regarding the remaining signals, these could be the residuals from the unreacted monomers or the initiators.

At the range of 1300cm^{-1} to 1000cm^{-1}, there were two strong signals present. From the range 1200cm^{-1} to 1100cm^{-1}, the peak at 1154cm^{-1} showed a decreasing trend in function of the SPMA molar% and the shape of the peak reduces from two spikes (100%, 75%, 50% SPMA) to one spike (25% and 0% SPMA). The normalised peak at wavenumber 1717cm^{-1} was a ester carboxyl stretch, whereby ester also exhibited peaks for symmetric or asymmetric $C-O-C$ stretch at 1050cm^{-1} to 1300cm^{-1} which was present in both SPMA and HEMA [36, 58]. The signal at 1040cm^{-1} as a doublet showed a similar trend, the observation indicated the presence of a functional group that only existed in hydrogels synthesised with SPMA monomer. From the article of Shislov and Kursan [60], a doublet of $O=S=O$ symmetric vibration would appear at 1033 to 1048cm^{-1}. In Figure 7, hydrogels with 100% SPMA molar% showed the highest intensity as a doublet peak. As the hydrogels were synthesised under different SPMA and HEMA ratio, the peak intensity was lowered and the shape changed from a double to a singlet. The quantification of signals at the sulfonate

group was graphed and explained in the appendix section 6.4.

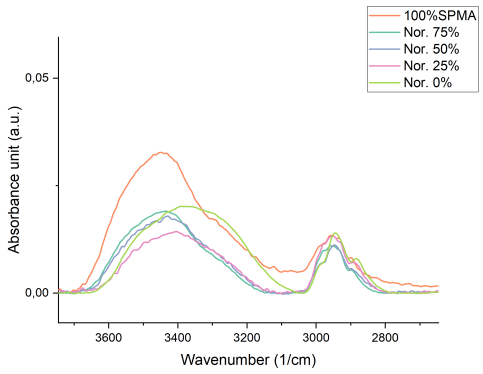

(a) Enlargement of wavenumber 3600cm^{-1} to 2800cm^{-1}

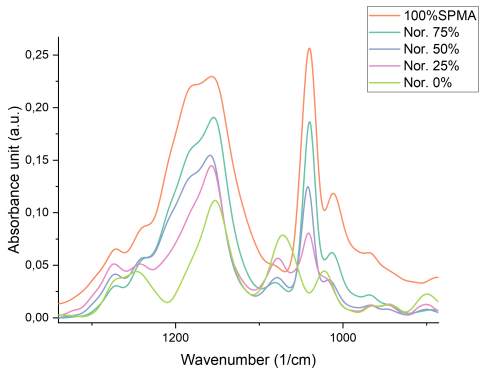

(b) Enlargement of wavenumber 1300cm^{-1} to 1000cm^{-1}

Figure 7: Enlargement of the interested regions. Figure (a) corresponds to the interaction of SO_3^- and/or hydroxyl group with water. Figure (b) corresponds to the SO_3^- vibration.

4.5 Scanning Electron Microscope (SEM)

The imaging of different SPMA molar% hydrogels surface morphology showed compact and lamellar structure, whereby the pores were only observable on the surface or on the cross section. There was no much literature reported on the copolymerization of SPMA and HEMA, and thus it was difficult to have a direct comparison of the SEM images. Therefore, the comparison would be focusing on literature that synthesised hydrogels using TEMED and APS as initiators, or MBA as crosslinker.

Starting the SEM images of 0% SPMA at 100μm scale, the structure was highly compact and it was not possible to observe any pores. At increasing the magnification and a scale bar of 10μm, there were polymer chains with particles along the chains, no evident pores were observed either. The reason for a lamellar structure of the hydrogels surface could be caused during the freezing step. Kaberova, Z. et al [61] reported morphological change of p(HEMA) during the transition from swollen state to solid state.

Connecting the compact surface with the low swelling ratio, the freeze-dried 0% molar% SPMA hydrogels were white and brittle. These results differed from the literature [36, 62] which interconnected pores (10–200μm in diameter) were observed. Hydrogels with larger SPMA molar% presented different degree of porosity and collapse of the network, but in general they were still less compact as 0% SPMA. 25% SPMA molar% hydrogels were an exception, these samples that showed clear pores on the cross-sectional area which explained the high swelling behaviour reported in section 4.2.

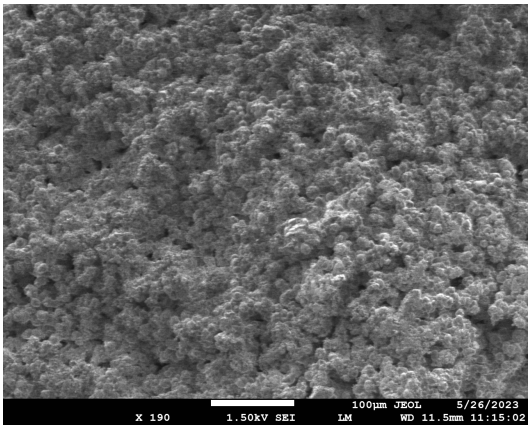

(a) 0% SPMA with scale bar 100μm

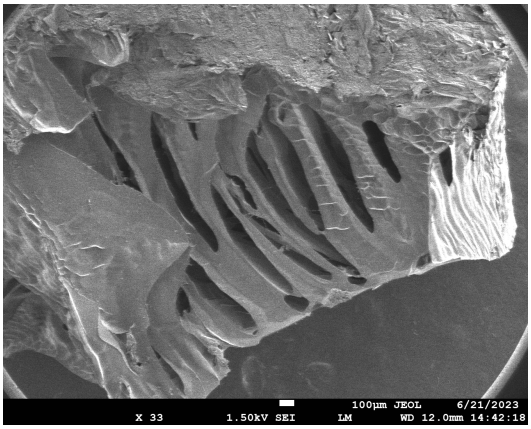

(b) 25% SPMA with scale bar 100μm

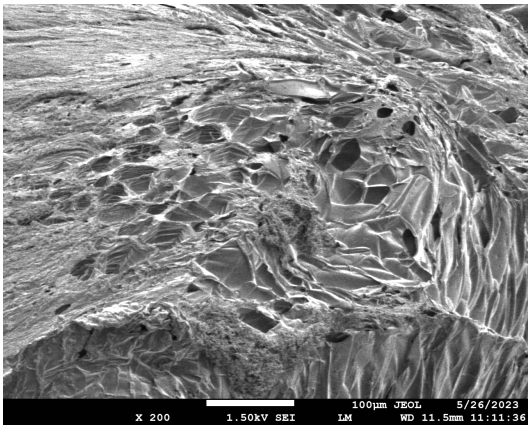

(c) 50% SPMA with scale bar 100μm

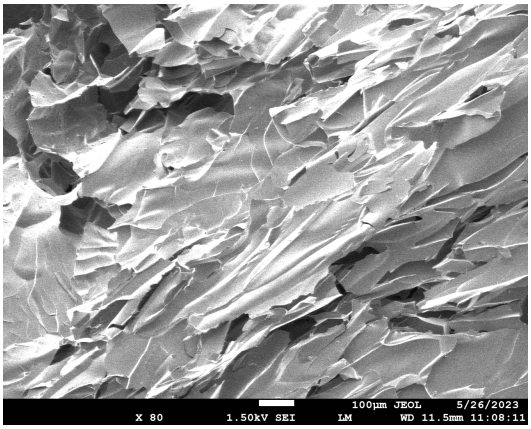

(d) 75% SPMA with scale bar 100μm

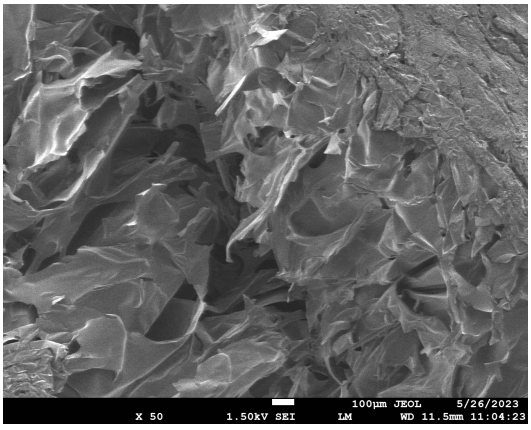

(e) 100% SPMA with scale bar 100μm

Figure 8: Image acquired with SEM technique

4.6 Confocal Laser Scanning Microscope (CLSM)

CLSM allowed imaging of hydrogels in the swollen state. Therefore, the freeze-dried hydrogels were immersed in 0.1mM Rhodamine B solution first. After 24 hours in the solution, a magenta colour was clearly visible in hydrogels under different SPMA molar%, meaning the Rhodamine B molecules had diffused into the network structure. The observed colour was intense for hydrogels of 100%, 75%, 50% and 25% SPMA composition. The 0% SPMA composition, however, presented a dim and less fluorescent colour. During the washing phase, the fluorescent colour in the hydrogels of 100%, 75%, 50% and 25% SPMA composition did not change after 4 to 5 days. Whereas the washing of 0 SPMA molar% hydrogels had a decreasing gradient of the colour intensity, the Rhodamine B continuous

diffusing out of the 0 SPMA molar% SPMA after being washed for 7 days.

The imaging of the swollen hydrogels using CLSM was successful, which the microscope allowed the visualisation of the charge distribution and the network structure with a magenta colour. The images were processed by adjusting the brightness/contrast, and certain regions-of-interest (ROIs) were selected to obtain the different light intensity emitted by the fluorophores.

In the images, both black and magenta colours were observed. The magenta colour corresponded to the charged polymer chains, because Rhodamine B was assumed to be attached to the negatively charges polymer chains. The black colour could be pores or p(HEMA), because HEMA is a neutral monomer. To verify the correspondence of the black colour, the reference hydrogels of 0 molar% SPMA were synthesised. The reference hydrogels were immersed in 0.1mM Rhodamine B solution and characterised using CLSM. The 3D structure of the reference hydrogels were reconstructed with Fiji Plugins function 3D Viewer and Volume Viewer. 3D viewer provided an overview of the structure, the image presented two colours: magenta and black. The hydrogels have a network structure comprising polymer chains/walls and pores, to find the correspondence of the colours to these structural part there were two scenarios.

1. There were SO_3^- pedants on the polymer backbone, and these anionic groups form electrostatic attraction with the cationic Rhodamine B molecules. Since Rhodamine B were the fluorescent molecules that emit light, the purple colour hence correspond to the polymer chains or walls.
2. The black colour could be either pores or p(HEMA). The reason is logical because there were no solid space for interaction. the option of p(HEMA) was due to the neutrality of the HEMA. However, the reference sample showed that the Rhodamine B still dyed the hydrogels because of osmotic pressure. Therefore, the black area represent the pores.

From the 3D Viewer, there was a clear distinction between the polymer walls/chains and the pores. The polymer walls/chains showed a magenta colour; whereas the pores had no colours. From the Volume Viewer, the intensity of the colour did not change much along the z-stack, whereas the black coloured area remained dark. Therefore, the dark colour represented the pores. Additionally, CLSM allowed investigation on the structure and the surface morphology of the hydrogels which implemented on the SEM images. The different hydrogels samples presented variations in the structure; nevertheless, there was no direct correlation between the SPMA molar% and the corresponding structure.

The charge distribution inside the hydrogels was represented by the magenta colour of Rhodamine B. In the Figure 9 the magenta colour was distributed evenly throughout the hydrogels network structure. Rhodamine B stained the polymer chains/walls, whereas the pores were dark. For the samples with different SPMA molar%, there were different degree of changes at the colour intensity along the z-stacks, and there were regions where the light was more intense than the others. During the CLSM image acquisition, the setting of the laser power and the gain were not constant for all the samples. Hence, it was not possible to compare the light intensity among the hydrogels synthesised under different SPMA molar%. For this reason, the light intensity was analysed with the measurement of the same sample. For instance, the light intensity of 25 molar% of SPMA was analysed by capturing different regions within the same sample. In this manner, there would be a fair comparison between the data, the images corresponding to each region were in 6.6. The images was processed following Fiji tutorial `https://imagej.net/imaging/image-intensity-processing`, specifically the sections *Brightness and Contrast* ,*Background correction*, and *Getting intensity values from multiple ROIs*.

The Figure 10 listed the change in light intensity. The intensity values were taken as the mean value of a region along the z-stacks. For 0% and 25% SPMA, there were an evident decreasing trend of the intensity as z-stacks was increasing. The reduction in light is due to a large uptake of water, which influenced the refractive light. For the other SPMA molar% compositions, the trends were not consistent and rather fluctuated along the z-stacks. The fluctuation was due to the intensity was a mean value from the region of interest, and in network structure there would be polymer chains/walls and pores. In the case that the regions of interest had a large change in the structure composition, it would influence the intensity, and thus causing fluctuation. The fluctuation was more pronounced

Figure 9: CLSM image of 0% SPMA

at 75% SPMA followed by 50%. During the washing phase (after the synthesis to remove unreacted monomers), the hydrogels composed by 50%, 75% and 100% molar% SPMA had different degree of fragmentation; whereas the 25% and 0% molar% SPMA hydrogels remained compact after long time immersed in water. The fragmentation of the hydrogels could depend on the concentration of the crosslinker and the physical interactions between the polymers. The physical interactions include hydrogen bonds and electrostatic attractions. At a lower SPMA molar% composition, thus higher HEMA molar% composition, the interaction of the hydrogen bond and the ionic attraction between sulfonate groups provided support to maintain the physical integrity of the hydrogels. Therefore, it was reasonable to have different intensity at each stack.

Additional to the distribution of the charges throughout the network, there were parts that the light with a higher intensity. As mentioned before, Rhodamine B is a positively charged molecule with the tendency to form electrostatic attraction [15] with the negatively charged polymer chains. The more intense parts could be explained as higher concentrated SPMA polymer chains. In other words, there could be a difference of polymerisation kinetics between the monomers such that one monomer reacted faster to cluster in the reaction mixture and the network skeleton of the copolymer. With this assumption, the more intense part would represent p(SPMA) whereby the polymerisation kinetics of the monomers had an influence on the structure of the hydrogels. However, this assumption could not be easily prove due to the lack of literature information regarding the copolymerization kinetics of the SPMA and HEMA monomers.

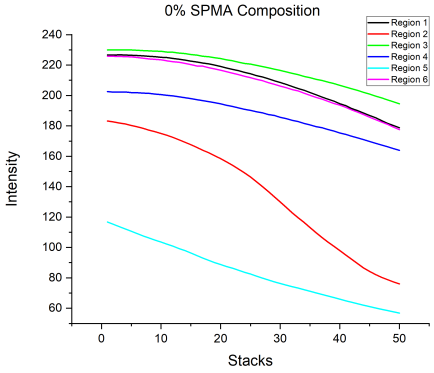

(a) 0% SPMA molar%

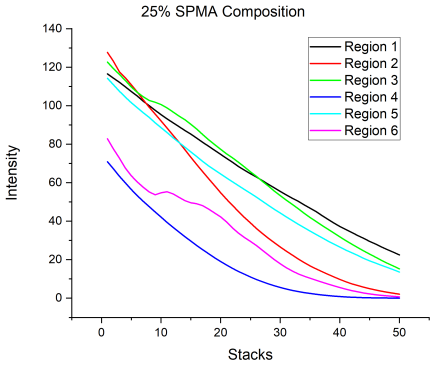

(b) 25% SPMA molar%

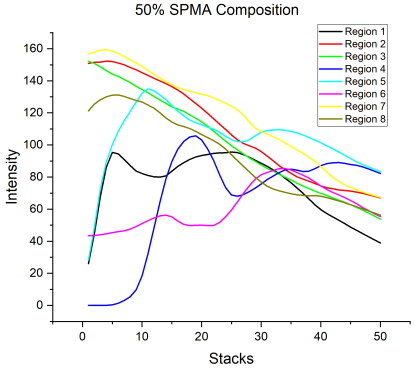

(c) 50% SPMA molar%

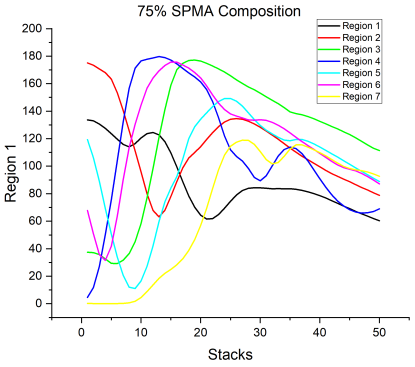

(d) 100% SPMA molar%

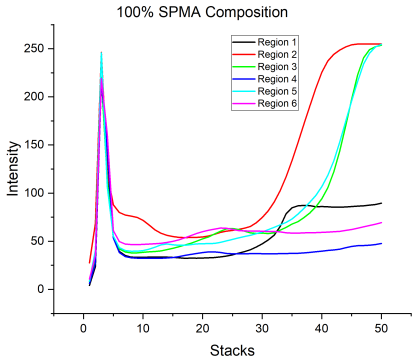

(e) 100% SPMA with scale bar 100μm

Figure 10: Light intensity under different SPMA molar%

5 Conclusion and Recommendation

The hydrogels synthesised under different SPMA and HEMA monomers molar ratio and characterised with swelling ratio, FTIR, optical microscope, SEM and CLSM. SPMA is a monomer of anionic character due to the group SO_3^-, which subsequently the synthesised hydrogels also had anionic pedant on the polymer backbone. The main focus of the research was to verify the feasibility of using CLSM to visualise the electric charge density inside the network structure. To further understand the influence of the sulfonate group on the charge density, hydrogels were synthesised under seven different SPMA and HEMA molar ratio.

The swelling ratio results suggested 100% and 25% SPMA composition had the highest swelling ratio, with an average value of 119.9281 g/g and 143.8925 g/g respectively. Even though these hydrogels had a different SPMA molar%, the swelling ratio was rather similar. The explanation for 100% SPMA was the substantial amount of sulfonate moieties inside the network structure, this point was proven by the optical microscope images. For 25% SPMA (75% HEMA), the addition of hydrophilic moieties in HEMA improved the swelling behaviour and increased the pore sizes as presented in SEM images.

In addition to swelling ratio, FTIR was applied to interpret the interaction of the sulphonate group and hydroxyl group with water. The FTIR spectrum showed signals at 1400cm^{-1}, this wavenumber is corresponds to sulfonate group SO_3^-. The signals at this wavenumber showed a decreasing trend along the reduction of SPMA molar%, and there was no peak for 0% SPMA. This indicated the influence of the SPMA molar ratio on the charge density. Furthermore, the signal at 3451cm^{-1} demonstrated that the interaction of the sulfonate group with the water was different from the hydroxyl group.

Based on these parameters, the swollen hydrogels dyed with Rhodamine B was characterised under CLSM. Rhodamine B is a positively charged fluorescent dye molecule that could form electrostatic attraction with the anionic hydrogels. In fact, the hydrogels immersed in the 0.1mM Rhodamine B presented a fluorescent pink colour. The colour intensity was similar among hydrogels of 100%, 75%, 50% and 25% SPMA composition, except for 0% SPMA that had a dim colour. During the washing phase to remove excessive dye inside the hydrogels, 0% SPMA had a continuous change in colour after 7 days in water. The characterisation of the dyed hydrogels in CLSM showed the charges were homogeneously distributed and the light intensity was decreasing along the z-stacks. To obtain quantitative information of the light intensity, the 3D reconstructed images were processed in Fiji. The light intensity was compared within the samples from the same SPMA molar%. The graph showed the a decrease trend in 0% and 25% SPMA, where the light was indeed reducing along the z-stack. The change of intensity for 0% SPMA was not as drastic as the 25% SPMA, the interpretation of the change was due to the difference in the swelling behaviour. 75% and 50% SPMA had a similar behaviour of decreasing light intensity despite some light fluctuation at the early z-stacks. The fluctuation could be interpreted as the structure of the hydrogels was fragmented, where light emitted by the fluorophores was not consistent. The degree of fragmentation increased at higher SPMA molar%, and thus the fluctuation was more pronounced with 75% SPMA than 50% SPMA. 100% SPMA showed an different behaviour, the intensity decreased at z-stack 9 and started increasing at z-stack 30. This observation indicated the structure of the hydrogels would influence the light intensity detection. At the more fragmented part the light would be brighter, whereas at the compact area the light would be dimmer.

In conclusion, the visualisation of the charge density using CLSM is a feasible method, the acquired images provided information such as the location of the charges, the intensity of the light along the z-stack, and the (3D) structure of the hydrogels. The influence of the SPMA molar% on the swelling behaviour was evident. The effect of the monomers molar ratio on the electric charge distribution was not possible due to different setting on the *ZEN* for each SPMA molar% image acquisition.

The recommendation on the CLSM characterisation is to maintain *ZEN* parameters such as laser power, gain, distance of z-stack to be constant for every sample measurement. Then the image acquisition would have the same conditions, and hence the influence of different SPMA molar% intensity would be comparable. For the quantitative intensity measurement, several regions were chosen for calculation. To have a overview of the entire 3D image, it is better to select the whole

area as one measurement, the results would yield one trend which ease the comparison. In addition, the measured intensity was influenced by the fragmentation. The was a lack of measurement of 100% SPMA, therefore the intensity behaviour could not be better analysed. Hence, it will be recommended to have at least three sample measurement for each monomer molar ratio.

The observation of the pores with SEM was not successful because of morphological changes during the drying step. Characterisation of hydrogels in the swollen state would provide true information regarding the morphology, literature [61, 63] suggested cryo-SEM imaging. This technique also has the potential to reveal the 3D structure of the hydrogels [63].

6 Appendix

6.1 Synthesised hydrogels

Here the images of the hydrogels at different stages were presented.

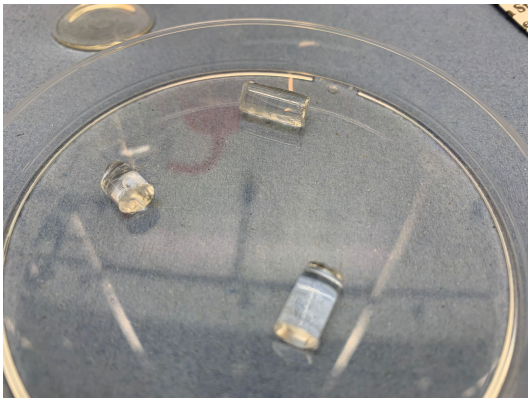

(a) 100% SPMA after 4 hours synthesis, transparent and rigid products

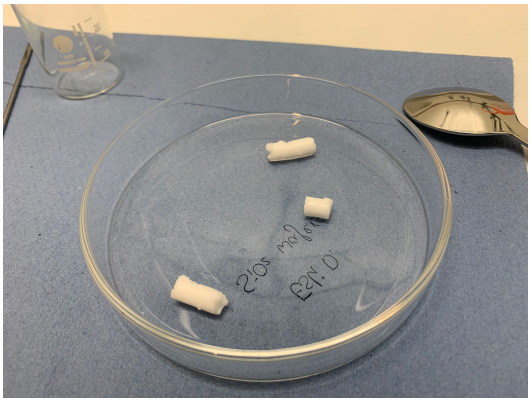

(b) 0% SPMA after 4 hours synthesis, white and flexible products

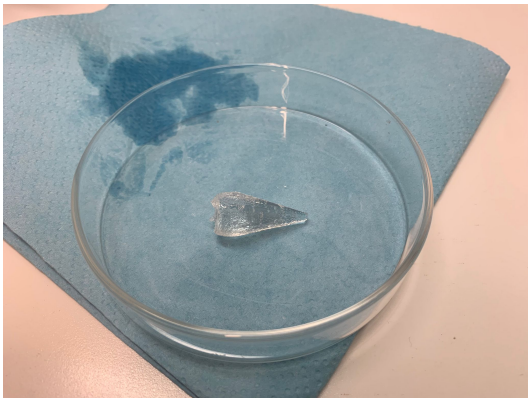

(c) 0% SPAM with 1:1 volume ratio of ethylene glycol and water, transparent and rigid products

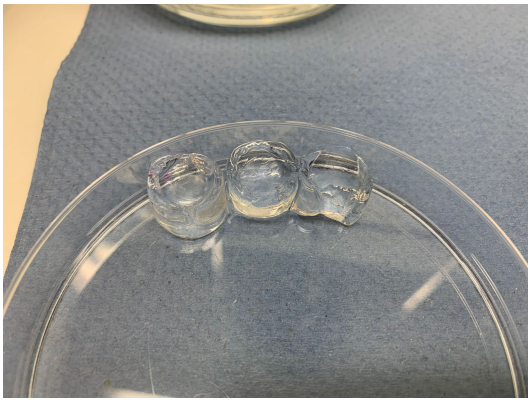

(d) The state of hydrogels after being washed for 24 hours

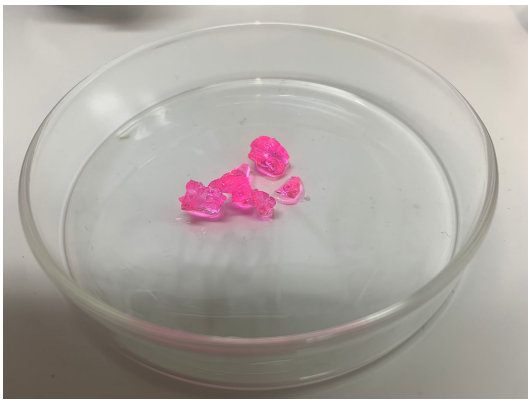

(e) 0% SPMA hydrogels dyed with 0.1mM Rhodamine B, the fluorescent pink colour is dimmer than 50%

(f) 50% SPMA hydrogels dyed with 0.1mM Rhodamine B, fluorescent pink colour

Figure 11

6.2 Swelling ratio of 0% SPMA trial synthesised hydrogels

This section recorded the trials to get a transparent 0% SPMA hydrogels.

Table 4: Results of the different trials. md = mass dry; mw = mass wet; Q = swelling ratio

Trials	md (g)	mw (g)	Q (g/g)	Average Q (g/g)
6.2.1	0.347	0.81817	0.47117	0.4067667
	0.302	0.70003	0.39803	
	0.22552	0.57662	0.3511	
6.2.2	0.05839	0.09757	0.03918	0.04661
	0.05551	0.10955	0.05404	
6.2.3	0.02365	0.0621	0.03845	0.0532
	0.04871	0.13988	0.09117	
	0.01805	0.04803	0.02998	
6.2.4	0.02444	0.07601	0.05157	0.056228
	0.03843	0.123354	0.084924	
	0.0143	0.04649	0.03219	
6.2.5	0.0153	0.03397	0.01867	0.0354867
	0.01943	0.04852	0.02909	
	0.03623	0.09493	0.0587	
6.2.6	0.07815	0.08354	0.00539	0.00456
	0.03169	0.03542	0.00373	

6.2.1 Replica of Liu. Q. et al

Liu, Q. et al reported [36] the synthesis of 0% SPMA with same materials listed in section 3 with the addition of TTC which is an agent for RAFT. For this project, control over the polymerisation was not relevant, hence TTC was excluded from the synthesis. The end products of this synthesis was soft and white.

Table 5: HEMA and MBA were dissolved in 7.0mL of water. The hydrogels were synthesised for 24 hours at 50℃.

Materials	Amount
HEMA (mL)	2.80
APS (g)	0.01
TEMED (mL)	0.1
MBA (g)	0.08

6.2.2 Repetition from Table 2 at 50℃

The synthesis was carried out the same manner as described in chapter **??**, with the addition of an oil bath at 50℃. During the synthesis, it was observed that the vial containing MBA turned white. The end products were white and soft, but the observation was dented for next synthesis trial.

6.2.3 Repetition from Table 2 alternating the material mixture

In this synthesis, the materials were mixed in a different vials. MBA, HEMA and water in one vial; the initiators in another vial. The idea was to prevent initiation of the crosslinker as observed in 6.2.3. The synthesis was at room temperature. however, no gelation occurred.

6.2.4 Repetition from Table 2 alternating the material mixture at 50℃

In this synthesis, the mixture was set in a 50℃ oil bath. Gelation occurred within 5 minutes, nevertheless the products were non-transparent.

6.2.5 Repetition from Table 2 without MBA

AS discussed in 6.2.1, it was observed that MBA started crosslinking yielding a white colour. Experiment 6.2.3 and 6.2.4 both failed, this trial synthesise without MBA at room temperature. Without MBA, HEMA should form physical crosslinking. The end products did not become transparent.

6.2.6 Synthesis using Table 2 with use of ethylene glycol

According to Kwok, A. [64], the phase behaviour of HEMA in water system has a ternary phase, such that HEMA solubility in water reduces as p(HEMA) increases. The addition of ethylene glycol would increase the transparency of the hydrogels. Thus, ethylene glycol was added to the synthesis, and the solution did not turn white in oil bath at 50℃. Transparent hydrogels were successfully synthesised.

6.3 Optical microscope

Images of 50% and 75% SPMA are listed here. The morphological properties of the hydrogels were observable.

6.3.1 50% SPMA

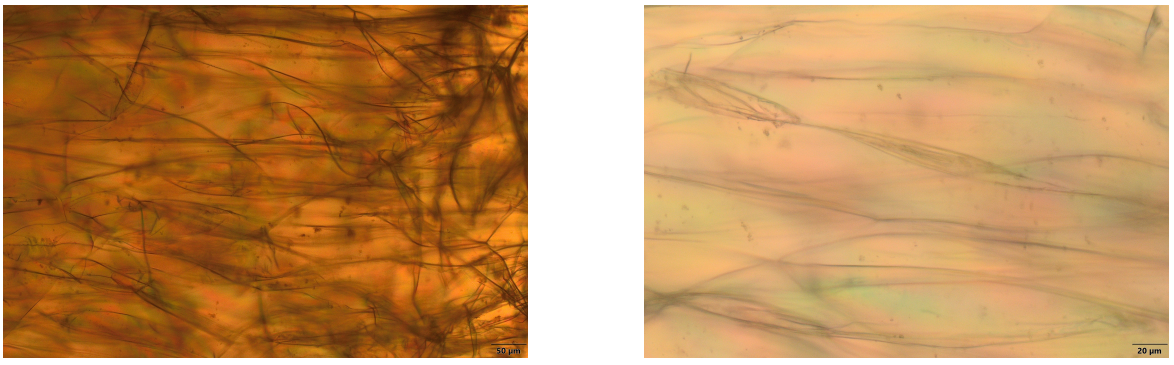

(a) Magnification 20x *(b) Magnification 50x*

Figure 12: The images showed the morphological characteristics for 50% SPMA

6.3.2 75% SPMA

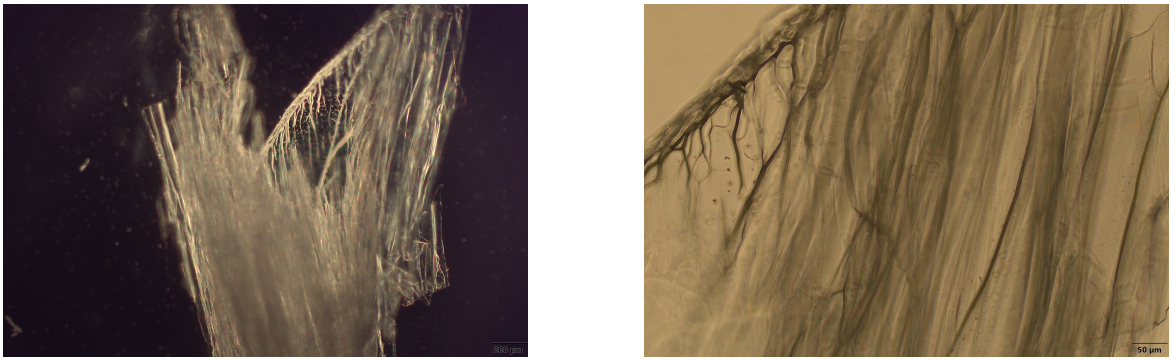

(a) Magnification 5x *(b) Magnification 50x*

Figure 13: 75% Water bubbles were observed at the translucent

6.4 FTIR

The absorbance unit is proportional to the SPMA molar%. Larger amount of SO_3^- pedants on the hydrogels polymer backbone at increasing SPMA molar%, and hence the absorbance is higher.

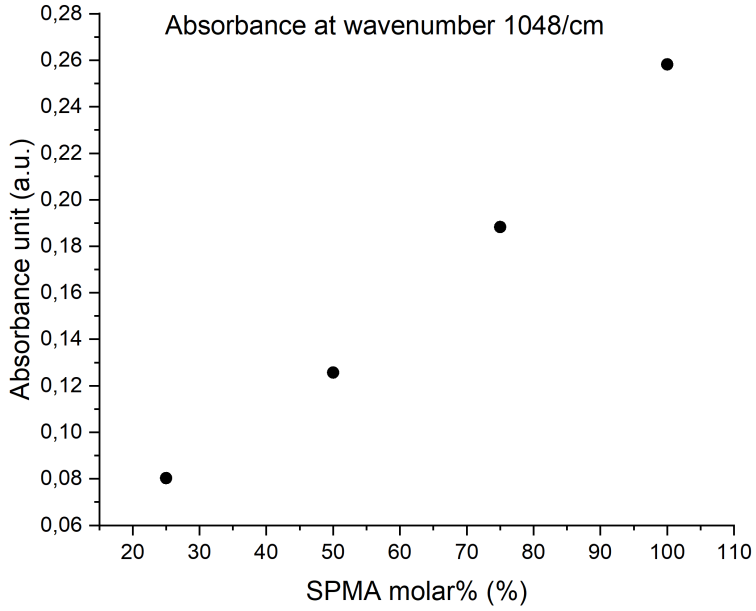

Figure 14: Absorbance at SO_3^- characteristic wavenumber 1048cm^{-1}.

6.5 CLSM

The images showed the structural differences, such as branches, pores, more intense strands.

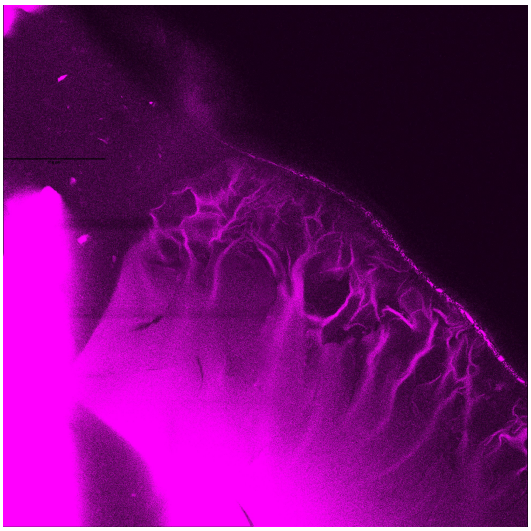

(a) 25% SPMA

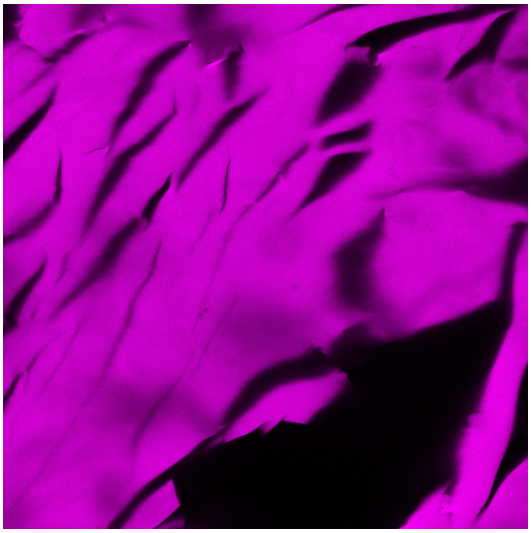

(b) 50% SPMA

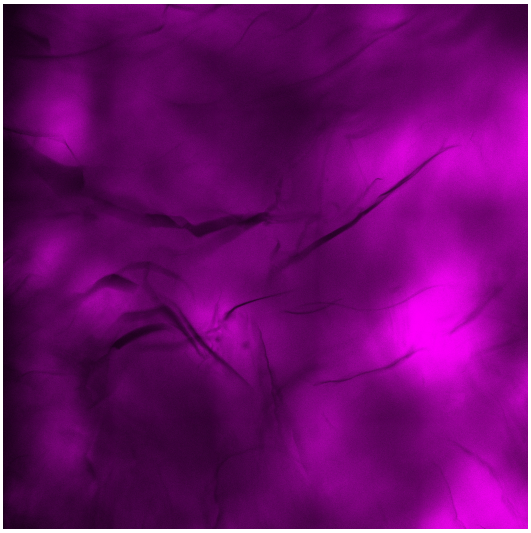

(c) 75% SPMA

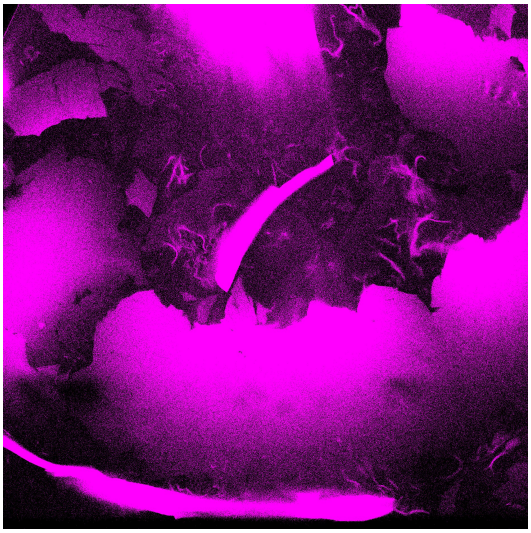

(d) 100% SPMA

6.6 Region selection for intensity measurement

The grey colour meant the background was subtracted such that intensity measurement was focused on the light emitted by Rhodamine B. Figure of 0% and 75% SPMA had the magenta colour because the grey colour image was lost. However, all the measurement was carried after subtracting the background light.

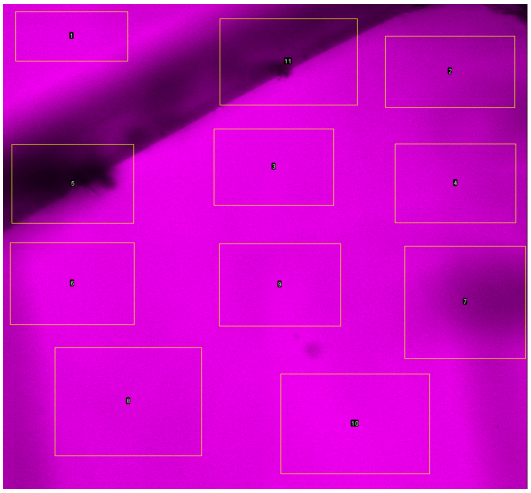

(a) 0% SPMA

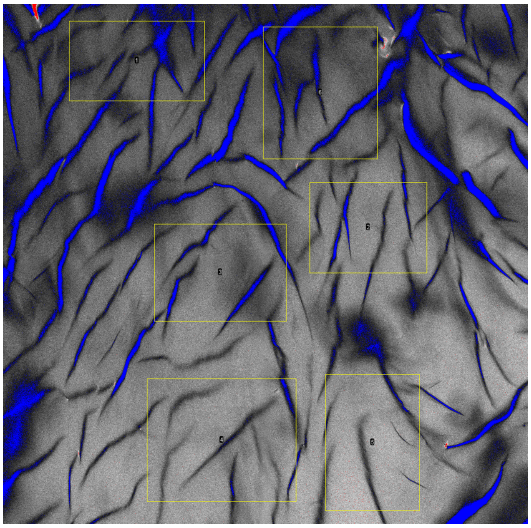

(b) 25% SPMA

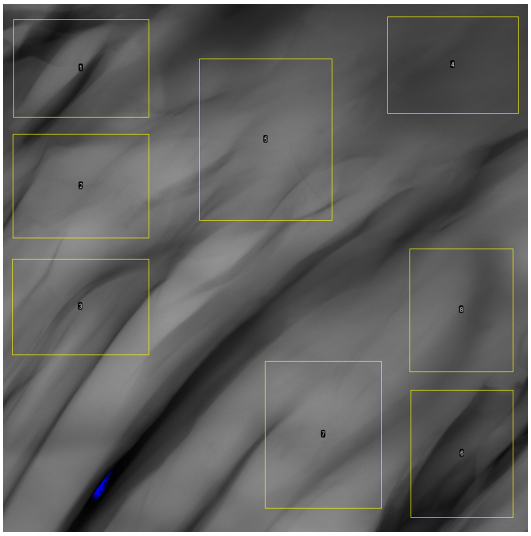

(c) 50% SPMA

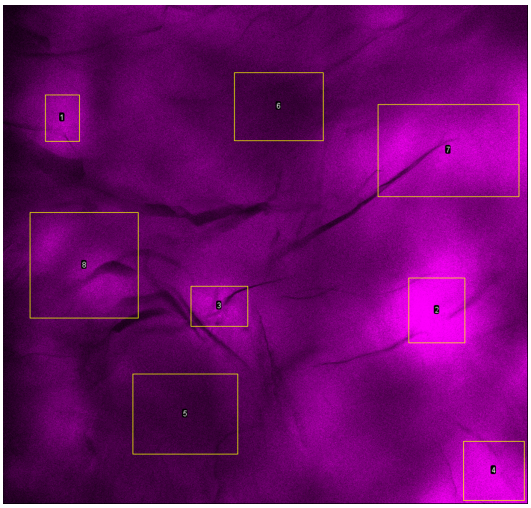

(d) 75% SPMA

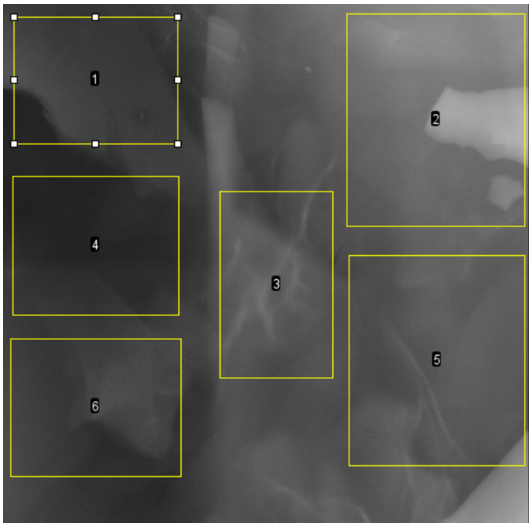

(e) 100% SPMA

Figure 16

References

[1] Hannah Ritchie and Max Roser and Pablo Rosado, “Energy,” 2022.

[2] N. G. M. S. R. B. Pandit, P., “Functionality and Properties of Bio-based Materials,” in *Bio-based Materials for Food Packaging*, 1st ed., Shakeel Ahmed, Ed. Singapore: Springer Link, 11 2018, pp. 83–103.

[3] J. Yi, X. Li, J. He, and X. Duan, “Drying efficiency and product quality of biomass drying: a review,” *Drying Technology*, vol. 38, no. 15, pp. 2039–2054, 2020. [Online]. Available: https://doi.org/10.1080/07373937.2019.1628772

[4] S. Stenström, “Drying of paper: A review 2000–2018,” *Drying Technology*, vol. 38, no. 7, pp. 825–845, 2020. [Online]. Available: https://doi.org/10.1080/07373937.2019.1596949

[5] H. S. EL-Mesery and S. E. El-khawaga, “Drying process on biomass: Evaluation of the drying performance and energy analysis of different dryers,” *Case Studies in Thermal Engineering*, vol. 33, p. 101953, 5 2022.

[6] C. C. F. M. M. F. O. O. N. A. W.-C. J. Hui Y. H., “3.4 Biomass Dryer,” pp. 73–75, 2008. [Online]. Available: https://app.knovel.com/hotlink/khtml/id:kt011EOTL4/food-drying-science-technology/biomass-dryer

[7] I. Alibas and A. Yilmaz, “Microwave and convective drying kinetics and thermal properties of orange slices and effect of drying on some phytochemical parameters,” *Journal of Thermal Analysis and Calorimetry*, vol. 147, no. 15, pp. 8301–8321, 2022. [Online]. Available: https://doi.org/10.1007/s10973-021-11108-3

[8] C. H. Scaman, T. D. Durance, L. Drummond, and D. W. Sun, “Combined Microwave Vacuum Drying,” *Emerging Technologies for Food Processing*, pp. 427–445, 1 2014.

[9] M. Marcotte and S. Grabowski, “Minimising energy consumption associated with drying, baking and evaporation,” *Handbook of Water and Energy Management in Food Processing*, pp. 481–522, 1 2008.

[10] U. S. K. Madduma-Bandarage and S. V. Madihally, “Synthetic hydrogels: Synthesis, novel trends, and applications,” *Journal of Applied Polymer Science*, vol. 138, no. 19, p. 50376, 2021. [Online]. Available: https://onlinelibrary.wiley.com/doi/abs/10.1002/app.50376

[11] S. Bashir, M. Hina, J. Iqbal, A. H. Rajpar, M. A. Mujtaba, N. A. Alghamdi, S. Wageh, K. Ramesh, and S. Ramesh, “Fundamental Concepts of Hydrogels: Synthesis, Properties, and Their Applications,” *Polymers*, vol. 12, no. 11, 2020. [Online]. Available: https://www.mdpi.com/2073-4360/12/11/2702

[12] S. J. Buwalda, K. W. Boere, P. J. Dijkstra, J. Feijen, T. Vermonden, and W. E. Hennink, “Hydrogels in a historical perspective: From simple networks to smart materials,” *Journal of Controlled Release*, vol. 190, pp. 254–273, 9 2014.

[13] A. K. Kaviti, J. Sri Ganesh Balaji, A. Siva Ram, and A. Aruna Kumari, “An overview on hydrogel materials for solar desalination,” *Materials Today: Proceedings*, vol. 44, pp. 2526–2532, 1 2021.

[14] S. W. Sharshir, A. M. Algazzar, K. A. Elmaadawy, A. W. Kandeal, M. R. Elkadeem, T. Arunkumar, J. Zang, and N. Yang, “New hydrogel materials for improving solar water evaporation, desalination and wastewater treatment: A review,” *Desalination*, vol. 491, p. 114564, 10 2020.

[15] J. Zhong, T. Zhao, and M. Liu, “Fluorescence microscopic visualization of functionalized hydrogels,” *NPG Asia Materials*, vol. 14, no. 1, p. 38, 2022. [Online]. Available: https://doi.org/10.1038/s41427-022-00376-6

[16] E. M. Ahmed, “Hydrogel: Preparation, characterization, and applications: A review,” *Journal of Advanced Research*, vol. 6, no. 2, pp. 105–121, 3 2015.

[17] Z. Zhang, H. Fu, Z. Li, J. Huang, Z. Xu, Y. Lai, X. Qian, and S. Zhang, “Hydrogel materials for sustainable water resources harvesting & treatment: Synthesis, mechanism and applications,” *Chemical Engineering Journal*, vol. 439, p. 135756, 7 2022.

[18] P. Sikdar, M. M. Uddin, T. M. Dip, S. Islam, M. S. Hoque, A. K. Dhar, and S. Wu, “Recent advances in the synthesis of smart hydrogels,” *Mater. Adv.*, vol. 2, no. 14, pp. 4532–4573, 2021. [Online]. Available: http://dx.doi.org/10.1039/D1MA00193K

[19] H. Luo, K. Wu, Q. Wang, T. C. Zhang, H. Lu, H. Rong, and Q. Fang, “Forward osmosis with electro-responsive P(AMPS-co-AM) hydrogels as draw agents for desalination,” *Journal of Membrane Science*, vol. 593, p. 117406, 1 2020.

[20] M. M. Rahman Md. Shirajur
}and Islam, I. M. Sazedul, Z. Asaduz, A. Tanvir, B. Shanta, S. Sadia, R. T. Ur, and R. M. Mizanur, “Morphological Characterization of Hydrogels,” in *Cellulose-Based Superabsorbent Hydrogels*, M. I. H. Mondal, Ed. Cham: Springer International Publishing, 2019, pp. 819–863. [Online]. Available: https://doi.org/10.1007/978-3-319-77830-3_28

[21] F. Rost, “Fluorescence Microscopy, Applications,” *Encyclopedia of Spectroscopy and Spectrometry*, pp. 627–631, 1 2017.

[22] K. Kolmakov, V. Belov, J. Bierwagen, C. Ringemann, V. Müller, C. Eggeling, and S. Hell, “Red-Emitting Rhodamine Dyes for Fluorescence Microscopy and Nanoscopy,” *Chemistry – A European Journal*, vol. 16, no. 1, pp. 158–166, 2010. [Online]. Available: https://chemistry-europe.onlinelibrary.wiley.com/doi/abs/10.1002/chem.200902309

[23] V. K. Thakur Sourbh
}and Thakur and A. O. Ademola, "History, Classification, Properties and Application of Hydrogels: An Overview," in *Hydrogels: Recent Advances*, M. K. Thakur Vijay Kumar
}and Thakur, Ed. Singapore: Springer Singapore, 2018, pp. 29–50. [Online]. Available: https://doi.org/10.1007/978-981-10-6077-9_2

[24] B. S. Kaith, A. Singh, A. K. Sharma, and D. Sud, "Hydrogels: Synthesis, Classification, Properties and Potential Applications—A Brief Review," *Journal of Polymers and the Environment*, vol. 29, no. 12, pp. 3827–3841, 2021. [Online]. Available: https://doi.org/10.1007/s10924-021-02184-5

[25] I. Capek, "Solution radical polymerization," *Nanocomposite Structures and Dispersions*, pp. 95–174, 1 2019.

[26] K. MATYJASZEWSKI and S. G. GAYNOR, "FREE RADICAL POLYMERIZATION," *Applied Polymer Science: 21st Century*, pp. 929–977, 1 2000. [Online]. Available: https://linkinghub.elsevier.com/retrieve/pii/B9780080434179500465

[27] Z. D. L. J. e. a. Gao, Y., "Complex polymer architectures through free-radical polymerization of multivinyl monomers," *Nat Rev Chem*, vol. 4, pp. 194–212, 2020.

[28] A. Rudin and P. Choi, "Free-Radical Polymerization," *The Elements of Polymer Science & Engineering*, pp. 341–389, 1 2013. [Online]. Available: https://linkinghub.elsevier.com/retrieve/pii/B9780123821782000080

[29] M. M. N. O. Koltzenburg, S., "Radical Polymerization ," in *Polymer Chemistry*. Berlin, Heidelberg: Springer, 12 2017, pp. 205–244.

[30] B. E. Obi, "Polymer Chemistry and Synthesis," *Polymeric Foams Structure-Property-Performance*, pp. 17–40, 1 2018.

[31] A. J. Scott and A. Penlidis, "Copolymerization," *Reference Module in Chemistry, Molecular Sciences and Chemical Engineering*, 1 2017. [Online]. Available: https://linkinghub.elsevier.com/retrieve/pii/B9780124095472139010

[32] M. A. Dubé, E. Saldívar-Guerra, and I. Zapata-González, "Copolymerization," *Handbook of Polymer Synthesis, Characterization, and Processing*, pp. 105–125, 2 2013. [Online]. Available: https://onlinelibrary.wiley.com/doi/full/10.1002/9781118480793.ch6https://onlinelibrary.wiley.com/doi/abs/10.1002/9781118480793.ch6https://onlinelibrary.wiley.com/doi/10.1002/9781118480793.ch6

[33] M. Mahinroosta, Z. Jomeh Farsangi, A. Allahverdi, and Z. Shakoori, "Hydrogels as intelligent materials: A brief review of synthesis, properties and applications," *Materials Today Chemistry*, vol. 8, pp. 42–55, 2018. [Online]. Available: https://www.sciencedirect.com/science/article/pii/S246851941730263X

[34] Y. Ebara Mitsuhiro
}and Kotsuchibashi, U. Koichiro, A. Takao, K. Young-Jin, N. Ravin, I. Naokazu, and H. J. M, "Smart Hydrogels," in *Smart Biomaterials*. Tokyo: Springer Japan, 2014, pp. 9–65. [Online]. Available: https://doi.org/10.1007/978-4-431-54400-5_2

[35] S. K. H. Gulrez, S. Al-Assaf, and G. O. Phillips, "Hydrogels: Methods of Preparation, Characterisation and Applications," in *Progress in Molecular and Environmental Bioengineering*, A. Carpi, Ed. Rijeka: IntechOpen, 2011, ch. 5. [Online]. Available: https://doi.org/10.5772/24553

[36] Q. Liu, X. Wen, S. Xu, P. Pi, J. Cheng, and R. Zeng, "Synthesis and properties of the antibacterial hydrogels with enhanced mechanical strengths," *Colloid and Polymer Science*, vol. 293, no. 6, pp. 1705–1712, 6 2015. [Online]. Available: https://link.springer.com/article/10.1007/s00396-015-3548-1

[37] F. Ganji, S. Vasheghani Farahani, and E. Vasheghani-Farahani, "Theoretical Description of Hydrogel Swelling: A Review," *Iranian Polymer Journal*, vol. 19, pp. 375–398, 6 2010.

[38] M. V. Dinu, M. Přádný, E. S. Drăgan, and J. Michálek, "Morphogical and swelling properties of porous hydrogels based on poly(hydroxyethyl methacrylate) and chitosan modulated by ice-templating process and porogen leaching," *Journal of Polymer Research*, vol. 20, no. 11, pp. 1–10, 10 2013. [Online]. Available: https://link.springer.com/article/10.1007/s10965-013-0285-3

[39] L. Sabbatini, "4.1 Principles of Fourier Transform Infrared Spectroscopy," in *Polymer Surface Characterization*. De Gruyter. [Online]. Available: https://app.knovel.com/hotlink/pdf/id:kt010RF3V2/polymer-surface-characterization/principles-fourier-transform

[40] S. Ebnesajjad, "Surface and Material Characterization Techniques," *Surface Treatment of Materials for Adhesive Bonding*, pp. 39–75, 1 2014.

[41] A. Di Gianfrancesco, "8 - Technologies for chemical analyses, microstructural and inspection investigations," in *Materials for Ultra-Supercritical and Advanced Ultra-Supercritical Power Plants*, A. Di Gianfrancesco, Ed. Woodhead Publishing, 2017, pp. 197–245. [Online]. Available: https://www.sciencedirect.com/science/article/pii/B9780081005521000087

[42] J. L. Nadeau and M. W. Davidson, "Optical Microscopy," *Characterization of Materials*, pp. 1–22, 10 2012. [Online]. Available: https://onlinelibrary.wiley.com/doi/full/10.1002/0471266965.com056.pub2https://onlinelibrary.wiley.com/doi/abs/10.1002/0471266965.com056.pub2https://onlinelibrary.wiley.com/doi/10.1002/0471266965.com056.pub2

[43] M. Wilson, J. DeRose, and C. Greb, "Microscope Resolution: Concepts, Factors and Calculation," 1 2023.

[44] M. W. Davidson and M. Abramowitz, "[Optical microscopy]." *Microscopica acta*, vol. 77 4, pp. 369–72, 2018.

[45] V. S. Raghuwanshi and G. Garnier, “Characterisation of hydrogels: Linking the nano to the microscale,” *Advances in Colloid and Interface Science*, vol. 274, p. 102044, 2019. [Online]. Available: https://www.sciencedirect.com/science/article/pii/S0001868619302477

[46] R. Schmitt, “Scanning Electron Microscope,” *CIRP Encyclopedia of Production Engineering*, pp. 1501–1505, 2019. [Online]. Available: https://link.springer.com/referenceworkentry/10.1007/978-3-662-53120-4_6595

[47] A. Canette and R. Briandet, “MICROSCOPY — Confocal Laser Scanning Microscopy,” *Encyclopedia of Food Microbiology: Second Edition*, pp. 676–683, 1 2014.

[48] R. Hard, J. Hipp, M. A. Tangrea, and J. E. Tomaszewski, “Applications of Image Science in Pathology and Cell Biology,” in *Pathobiology of Human Disease*, L. M. McManus and R. N. Mitchell, Eds. San Diego: Academic Press, 2014, pp. 3723–3759. [Online]. Available: https://www.sciencedirect.com/science/article/pii/B9780123864567072038

[49] J. Sanderson, “Confocal Microscopy,” in *Principles of Light Microscopy: From Basic to Advanced*, V. Nechyporuk-Zloy, Ed. Cham: Springer International Publishing, 2022, pp. 105–138. [Online]. Available: https://doi.org/10.1007/978-3-031-04477-9_5

[50] A. Elliott, “Confocal Microscopy: Principles and Modern Practices ,” *Current protocols in cytometry*, vol. 92, no. 1, 3 2020.

[51] J. Jonkman, C. M. Brown, G. D. Wright, K. I. Anderson, and A. J. North, “Tutorial: guidance for quantitative confocal microscopy,” *Nature Protocols*, vol. 15, no. 5, pp. 1585–1611, 2020. [Online]. Available: https://doi.org/10.1038/s41596-020-0313-9

[52] M. Fontana, Y. Li, P. Dunipace, T. W. Noblitt, G. Fischer, B. P. Katz, and G. K. Stookey, “Measurement of enamel demineralization using microradiography and confocal microscopy. A correlation study,” *Caries research*, vol. 30, no. 5, pp. 317–325, 1 1996. [Online]. Available: https://pubmed.ncbi.nlm.nih.gov/8877084/

[53] H. Omidian, K. Park, U. Kandalam, and J. G. Rocca, “Swelling and Mechanical Properties of Modified HEMA-based Superporous Hydrogels,” *Journal of Bioactive and Compatible Polymers*, vol. 25, no. 5, pp. 483–497, 2010. [Online]. Available: https://doi.org/10.1177/0883911510375175

[54] W. Tu, P. Maksym, K. Kaminski, K. Chat, and K. Adrjanowicz, “Free-radical polymerization of 2-hydroxyethyl methacrylate (HEMA) supported by a high electric field,” *Polymer Chemistry*, vol. 13, no. 19, pp. 2850–2859, 5 2022. [Online]. Available: https://pubs.rsc.org/en/content/articlehtml/2022/py/d2py00320ahttps://pubs.rsc.org/en/content/articlelanding/2022/py/d2py00320a

[55] T.-Y. Chen, Y.-J. Jiang, and H.-W. Chien, “Developing Transparent and Conductive PolyHEMA Gels Using Deep Eutectic Solvents,” *Polymers*, vol. 15, no. 12, 2023. [Online]. Available: https://www.mdpi.com/2073-4360/15/12/2605

[56] A. R. Hernández-Martínez, C. Silva-Cuevas, D. Rangel-Miranda, and J. A. Lujan-Montelongo, “Adsorption and swelling studies of 2-hydroxyethyl methacrylate- and N,N-dimethylacrylamide-based porous copolymers and their possible applications for QCM-sensors,” *Applied Surface Science*, vol. 572, p. 151508, 1 2022.

[57] B. Yilmaz and O. Ozay, “Synthesis, Characterization and Biomedical Applications of p(HEMA-co-APTMACl) Hydrogels Crosslinked with Modified Silica Nanoparticles,” *Biointerface Research in Applied Chemistry*, vol. 12, pp. 3664–3680, 6 2022.

[58] M. F. Passos, D. R. C. Dias, G. N. T. Bastos, A. L. Jardini, A. C. B. Benatti, C. G. B. T. Dias, and R. Maciel Filho, “pHEMA hydrogels,” *Journal of Thermal Analysis and Calorimetry*, vol. 125, no. 1, pp. 361–368, 2016. [Online]. Available: https://doi.org/10.1007/s10973-016-5329-6

[59] M. Pocheć, K. M. Krupka, J. J. Panek, K. Orzechowski, and A. Jezierska, “Intermolecular Interactions and Spectroscopic Signatures of the Hydrogen-Bonded System—n-Octanol in Experimental and Theoretical Studies,” *Molecules*, vol. 27, no. 4, 2 2022. [Online]. Available: /pmc/articles/PMC8878718//pmc/articles/PMC8878718/?report=abstracthttps://www.ncbi.nlm.nih.gov/pmc/articles/PMC8878718/

[60] N. M. Shishlov and S. L. Khursan, “Effect of ion interactions on the IR spectrum of benzenesulfonate ion. Restoration of sulfonate ion symmetry in sodium benzenesulfonate dimer,” *Journal of Molecular Structure*, vol. 1123, pp. 360–366, 2016. [Online]. Available: https://www.sciencedirect.com/science/article/pii/S0022286016306056

[61] Z. Kaberova, E. Karpushkin, M. Nevoralová, M. Vetrík, M. Šlouf, and M. Dušková-Smrčková, “Microscopic Structure of Swollen Hydrogels by Scanning Electron and Light Microscopies: Artifacts and Reality,” *Polymers*, vol. 12, no. 3, 2020. [Online]. Available: https://www.mdpi.com/2073-4360/12/3/578

[62] I. Perçin, E. Aksöz, and A. Denizli, “Gelatin-Immobilised Poly(hydroxyethyl methacrylate) Cryogel for Affinity Purification of Fibronectin,” *Applied Biochemistry and Biotechnology*, vol. 171, no. 2, pp. 352–365, 2013. [Online]. Available: https://doi.org/10.1007/s12010-013-0352-6

[63] M. Koch and M. K. Włodarczyk-Biegun, “Faithful scanning electron microscopic (SEM) visualization of 3D printed alginate-based scaffolds,” *Bioprinting*, vol. 20, p. e00098, 12 2020.

[64] A. Y. Kwok, G. G. Qiao, and D. H. Solomon, “Synthetic hydrogels 3. Solvent effects on poly(2-hydroxyethyl methacrylate) networks,” *Polymer*, vol. 45, no. 12, pp. 4017–4027, 5 2004.